Distribution Agreement

In presenting this thesis or dissertation as a partial fulfillment of the requirements for an advanced degree from Emory University, I hereby grant to Emory University and its agents the non-exclusive license to archive, make accessible, and display my thesis or dissertation in whole or in part in all forms of media, now or hereafter known, including display on the world wide web. I understand that I may select some access restrictions as part of the online submission of this thesis or dissertation. I retain all ownership rights to the copyright of the thesis or dissertation. I also retain the right to use in future works (such as articles or books) all or part of this thesis or dissertation.

Signature:

_____ _____

Peng Guo Date

Lifetime Resolved Fluorescence Correlation Spectroscopy and Two-Photon Spectroscopy of Amyloid Nanotube Bundles

By

Peng Guo

Doctor of Philosophy

Physics

_____
Keith Berland, Ph.D.
Advisor

_____
David Dunlap, Ph.D.
Committee Member

_____
Laura Finzi, Ph.D.
Committee Member

_____
Ivan Rasnik, Ph.D.
Committee Member

_____
Kurt Warncke, Ph.D.
Committee Member

_____
Eric Weeks, Ph.D.
Committee Member

Accepted:

_____
Lisa A. Tedesco, Ph.D. Dean of the Graduate School

_____
Date

Lifetime Resolved Fluorescence Correlation Spectroscopy and Two-Photon Spectroscopy of Amyloid Nanotube Bundles

By

Peng Guo

B.S., University of Science and Technology of China, 2004

Advisor: Keith Berland, Ph.D.

An abstract of

A dissertation submitted to the Faculty of the Graduate School of Emory University

in partial fulfillment of the requirements for the degree of Doctor of Philosophy

in Physics

2009

Abstract

Lifetime Resolved Fluorescence Correlation Spectroscopy and Two-Photon Spectroscopy of Amyloid Nanotube Bundles

By Peng Guo

Fluorescence correlation spectroscopy (FCS) has been widely used to investigate molecular dynamics and interactions in biological systems. However, these diffusion based assays currently have a major limitation, which requires that the diffusion coefficients of component species in a sample must be substantially different in order to be resolved. This limitation can be overcome, and the resolution of FCS measurements can be enhanced, by combining FCS measurements with measurements of fluorescence lifetimes. We show that we can dramatically enhance resolution in FCS measurements using global analysis on simultaneously acquired FCS and lifetime data. The method accurately resolves the concentration and diffusion coefficients of multiple sample components, even when their diffusion coefficients are identical, provided that there is a difference in the lifetime of the component species. We show examples of this technique by using both simulations and experiments. It is expected that this method will be of significance for a broad range of researchers studying molecular interactions. In a separate project, a potentially useful amyloid nanotube bundle material from the β-amyloid proteins is studied. We used two-photon excited fluorescence (TPEF) and second harmonic generation (SHG) to investigate the photophysical properties of this material. The emission properties of the bundles are characterized, and their dependence on the moisture level is revealed. The mechanism of the intrinsic fluorescence is discussed to be related to the electron delocalization within the peptides. The spectroscopic and microscopic study of the amyloid nanotube bundles may open up interesting new perspectives in the bio-inspired material science area.

Lifetime Resolved Fluorescence Correlation Spectroscopy and Two-Photon Spectroscopy of Amyloid Nanotube Bundles

By

Peng Guo

B.S., University of Science and Technology of China, 2004

Advisor: Keith Berland, Ph.D.

A dissertation submitted to the Faculty of the Graduate School of Emory University in partial fulfillment of the requirements for the degree of Doctor of Philosophy in Physics

2009

Acknowledgements

I would like to thank

Keith Berland, my advisor, for his support in the past three and half years and for his valuable advice, patience and enthusiasm throughout my graduate study at Emory. His scientific guidance and insights made me more mature in scientific thinking, which will be a treasure for life.

Ivan Rasnik for his mentoring and teaching during my second rotation from Dec, 2005 to May, 2006, and his continuing guidance over the years.

Kurt Warncke, Eric Weeks, Laura Finzi and David Dunlap for their helpful input in my research and being supportive over the years.

All the former and current members of Biophotonics lab including Suzette Pabit, Jianrong Wu, Yumei Yan, Zhiyong Dong, Neil Anthony and Keon-young Park for their help and encouragements over the years. I want to particularly thank Suzette Pabit for her mentorship in my first rotation period in the lab and the collaboration in the Nab2 project; Neil Anthony for his contribution in the Igor software coding of my LFCS project and his handy image acquisition software.

Seth Kelly and Anna Bramley for preparing eGFP and Nab2 for me and teaching me protein purification techniques.

Yan Liang for collaborating on the amyloid's lifetime project and preparing amyloid nanotube bundles for me.

Songli Xu and Maureen Powers for teaching me immunofluorescence technique.

Boi Hanh (Vincent) Huynh for his encouragements and wise advices over the years.

Virginia Shadron from graduate school for her support, encouragement and valuable advice about life.

Edmund Day for his mentorship and encouragements when I first gave lectures of Introductory Physics 141 to 300+ undergraduates.

Raymond DuVarney for helping me with the Chinese Student Union at Emory (CSUE) activities.

Jonathan Carr and Art Kleyman for their help on the network issues and detector power supply issues.

All the people in Physics department that enriched my life at Emory, including Wesley Robertson, Jessica Hernandez-Guzman, Jin Ha Kim, Kazem Edmond, Julie Coats, Trent Brunson, Adonis Bovell, Annika Kriisa, Jakub Otwinowski, Yuyen Lin, Miao Wang, Li Sun, Chen Zhu, Haowei Wang, Dandan Chen, Qing Shao, Hanlin Chen and all the other faculty, staff and students.

Most of all, I want to dedicate this achievement to my wonderful parents Baosheng Guo and Lili Zhang for their unconditioned love and support. Without them, I would not achieve what I have achieved.

Table of Contents

List of Figures

List of Tables

Chapter 1 Introduction of Scope

One of the major goals in biological sciences is to understand how particular cellular processes occur. The knowledge of a cellular process such as nuclear transport requires substantial understanding of corresponding molecular interactions and dynamics during that process. Various experimental methods have been developed and improved to address how molecules interact. Imaging methods like Atomic Force Microscopy (AFM) (García et al., 2002, Butt et al., 2005), Scanning Tunneling Microscopy (STM) (Hansma et al., 1987, Frommer, 1992) and cryo-Transmission Electron Microscopy (cryo-TEM) are used to study conformations of single molecules, to investigate the interaction and complex-formation of molecules. Other optical methods like fluorescence microscopy and spectroscopy give new insights in the motion and mobility of molecules. Fluorescence techniques allow observing interactions and dynamics with high accuracy and precision, either in solution or inside cells. Such studies of molecular interactions are first steps towards the understanding of basic biological questions involving molecular interactions.

Over the last two decades, fluorescence spectroscopy and microscopy has seen great advance in applications in biology. Due to its noninvasive nature coupled with high temporal and spatial resolution and superior sensitivity, fluorescence spectroscopy and microscopy becomes an integrated part of biological and biomedical investigations. A search using the key word fluorescence and molecular interactions through ISI web of science returns the number of papers published in the past three decades.

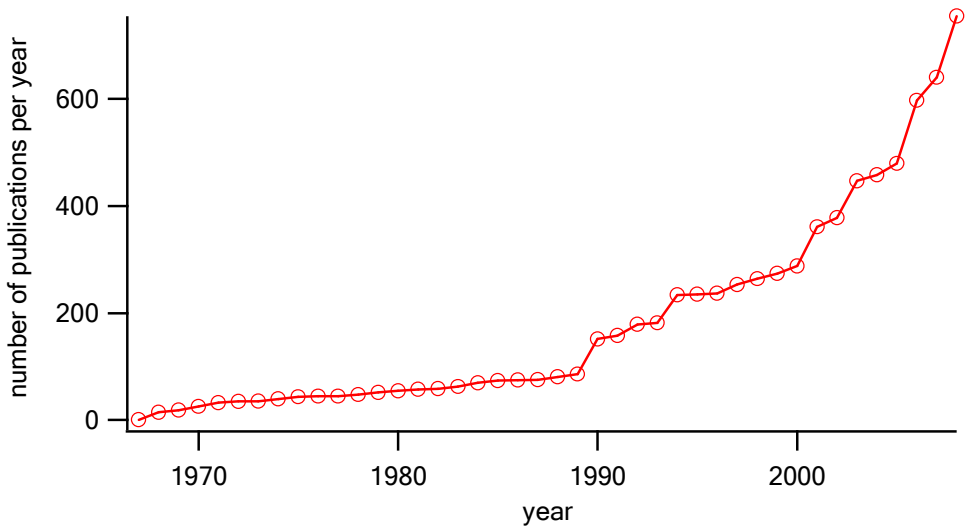

Figure 1.1: search results on fluorescence and molecular interactions from web of science http://apps.isiknowledge.com . Applications of fluorescence techniques have seen an exponential increase in studying molecular interactions.

The dramatic increase of publications shows the rapidly growing interests and applications in the fluorescence techniques. Among many fluorescence-based techniques, fluorescence correlation spectroscopy (FCS) and fluorescence lifetime are two techniques that have gained significant attentions due to their remarkable ability of studying dynamics and interactions at the molecular level.

In the first part of my thesis, I developed a new methodology of combining fluorescence correlation spectroscopy and fluorescence lifetime technique, aiming to reveal the potential of the combination of FCS and lifetime in resolving multiple species from a heterogeneous system that offers unprecedented accuracy compared to standard FCS or lifetime analysis. We have used both simulations and experiments to thoroughly investigate its application and limitation range. The future steps may include applications in the living cells to investigate molecular dynamics and interactions *in vivo*.

In the second part, utilizing the newly found intrinsic fluorescence phenomenon, I investigated the photophysical properties of the nanotube bundles formed by amyloid peptides through Two-Photon Excited Fluorescence (TPEF) and Second Harmonic Generation (SHG) technique. The intrinsic fluorescence and SHG signal could open up new areas in the bio-inspired material science.

In short, Chapter 2 introduces a novel methodology of resolving multiple-component system that combines the FCS and lifetime analysis. Chapter 3 discusses the newly discovered intrinsic fluorescence in amyloid bundles. These materials were not known to have intrinsic fluorescence signals, and we used a combination of spectroscopic and microscopic methods to characterize the photophysical properties of the materials.

Chapter 2 Lifetime-Resolved Fluorescence Correlation Spectroscopy

2.1 Summary

Molecular interactions such as protein-nucleic acid interactions determine the fate of DNA replication, transcription and translation, and thus a fundamental topic in life sciences and have been extensively studied. As a powerful tool for studying molecular interactions, fluorescence correlation spectroscopy (FCS) has been widely used in a binding assay to study molecular interactions. FCS technique quantifies species based on diffusion coefficient of individual species, however, a substantial difference in the magnitude of the diffusion coefficient is required to determine each species' concentration accurately. Furthermore, when the two species'

brightnesses are different, the quantification of individual species would be further obscured. This heavily limits the use of FCS in studying molecular interactions.

In this chapter, we introduce a new multi-dimensional fluorescence spectroscopy that combines fluorescence correlation spectroscopy (FCS) and fluorescence lifetime analysis to achieve enhanced resolvability of species from mixtures. Our proposed technique globally links the concentration and molecular brightness across FCS and lifetime analysis and quantifies fluorescent species on the basis of both their specific diffusion coefficient and excited-state lifetime. We show with simulations and experiments that the new method not only overcomes the hurdle of requiring substantial difference in diffusion coefficient and molecular brightness by FCS, but also provide superior accuracy in determining each species' concentration, diffusion coefficient, molecular brightness and excited-state lifetime, compared to existing FCS or lifetime technique. The statistical accuracy in characterizing each species in terms of concentration, molecular brightness, diffusion coefficient and excited-state lifetime is also presented in this paper. It is expected that this novel method will be of significance for studying molecular interactions, for example, protein-nucleic acid binding or protein assembly in life sciences.

2.2 Introduction

Biological systems in nature are indeed composed of multiple biomolecular components, such as various proteins and nucleic acids. They interact or assemble to perform proper biological functions; thus, the ability to indentify and quantify individual species from a multi-component mixture is crucial for understanding the interactions thus functions of individual components of biological systems in life sciences.

Fluorescence-based techniques provide unique accuracy and flexibility to study biological systems, thus have been widely applied to a variety of biochemical and biophysical areas (Lakowicz, 2006a). The first fluctuation-based fluorescence method, fluorescence correlation spectroscopy (FCS) was developed to quantify interactions of biomolecules (Elson et al., 1974, Magde et al., 1974) and has been further developed in the subsequent three decades. FCS is a technique with single molecule sensitivity that analyzes the fluctuations in fluorescence intensity within a tiny volume (≈ fL) that are caused by the changes in the number or brightness of the fluorophores inside the detection volume. The processes behind this involves particle motion (diffusion or transport) into and out of the detection volume, and/or photochemical and photophysical processes. The ability to monitor those changes makes FCS an excellent technique for the investigation of dynamic processes of biomolecules. As a result, FCS has been used to measure diffusion coefficients (Koppel et al., 1976), fluorophore concentrations, particle sizes, chemical reactions (Magde, 1976), protein oligomerization (Berland et al., 1996), DNA conformational changes (Kral et al., 2002, Wennmalm et al., 1997), and binding/unbinding processes (Kelly et al., 2007), among others (Elson, 2001, Berland et al., 1995, Hess et al., 2001).

Fluorescence lifetime analysis is another widely used fluorescence technique and has also proven to be one of the most reliable approaches to measure molecular interactions in vitro (Lakowicz, 2006a). With the advent of fluorescence proteins, fluorescence lifetime analysis has become more widely used for detecting protein-protein interactions in living cells (Bastiaens et al., 1999). Other techniques including fluorescence anisotropy are developed to probe the interactions of biomolecules as well (Visser et al., 1999, Steiner, 1991, Volkmer et al., 2000, Gough et al., 1993). Although these techniques, exemplified by FCS and fluorescence lifetime analysis, have made tremendous progress in life sciences, there exist limitations of each of them that have been difficult to obtain further unambiguous results to many important biological questions. For example, fluorescence lifetime analysis is able to resolve the intensity fraction of more than one

molecular species from a multi-component system based on species' different lifetime values; however, real concentrations of molecules are not possible to be obtained, therefore fluorescence lifetime analysis is not applicable in cases when concentrations of molecules are desired. In the case of FCS, in order to resolve more than one species from a mixture by FCS, FCS relied on using the different diffusion coefficients of species to separate each component species and provide information regarding concentration, diffusion coefficient and molecular brightness, however, a minimum 1.6 of diffusion coefficient ratio is required to apply FCS (Meseth et al., 1999). Because the diffusion coefficient scales with hydrodynamics radius R of respective fluorophore, $D = kT / 6\pi\eta R$, where D is the diffusion coefficient, η is the viscosity of the medium, T is the medium temperature, assuming globular shape, a 5-8 fold difference in molecular weight of two species is needed to fulfill the requirement. Although there are cases that meet this requirement, the limitation of single-color FCS resolvability based on diffusion coefficient is quite obvious. What is more, in a heterogeneous sample, when one species labeled with fluorophores interacts with another species, not only the molecular weight of the complex changes, photophysical properties of the complex including molecular brightness and lifetime often change too.

In the past, this change of molecular brightness in fluorescent species has not been carefully studied, instead, this change has often been assumed to be negligible or to a guessed value, as will be discussed in this thesis, this assumption about molecular brightness yields erroneous results in FCS analysis under most circumstances. Further technical developments of existing FCS analysis are therefore highly desired. In response to this difficulty in resolving biomolecules of similar molecular weight, other techniques including Photon Counting Histogram (PCH) (Chen et al., 1999, Muller et al., 2000) and Time-integrated Fluorescence Cumulant Analysis (TIFCA) (Wu et al., 2005) have been proposed. PCH technique resolves multiple molecular species based on their

different molecular brightness, and has been used to study molecular concentrations in solution (Chen et al., 2002) and protein oligomerizations in vitro (Chen et al., 2003). Nonetheless, PCH doesn't provide the dynamics information about the molecular species and is constrained by the assumption that diffusion of molecules occurs in a longer time scale than the sampling time of data acquisition. TIFCA is another powerful technique that is able to resolve mixtures based on components' diffusion coefficient and brightness (Wu et al., 2005, Wu et al., 2006), but it heavily relies on using molecular brightness to separate two species. When more than one fluorescent component possesses similar molecular brightness, the usefulness of TIFCA is limited.

Global fitting algorithms have been shown to dramatically increase the accuracy of analysis, both global analysis of FCS and lifetime data have been reported to effectively increase the resolution of concentration and diffusion time of molecular species in solution (Skakun et al., 2005, Barber et al., 2005) and have been used to study the interaction of biomolecues (Barber et al., 2005, Grecco et al., 2009). Due to the large number of coefficients that need to be optimized simultaneously, providing more constraints in fitting would increase the optimization tremendously, generating fewer errors for different parameters. It was shown that the global analysis of lifetime provides sufficient information to resolve a bi-exponential decay model, and that accuracy and precision of the estimated parameters could be increased significantly. However, the minor component in a two-component system can only be estimated from the fractional count rates, which is the product of concentration and brightness, therefore, the overall intensity ratio rather than absolute concentrations are revealed. However, when a heterogeneous biological system is studied, the real concentration of each component is often desired.

Here, we proposed a new methodology – Lifetime Resolved Fluorescence Correlation Spectroscopy (LFCS) to overcome the limitations set by FCS and fluorescence lifetime analysis. LFCS globally link FCS and lifetime model and analyze FCS and lifetime data simultaneously.

This new LFCS analysis combines the temporal analysis of FCS at sub-millisecond time scale and the lifetime analysis at nanosecond time scale. It is not only able to obtain diffusion, lifetime, and brightness information of a multi-component system all in one measurement; LFCS also possesses greater sensitivity and accuracy than individual FCS or FLIM analysis. LFCS will be powerful in circumstances when individual techniques are not sensitive enough to resolve molecular species. In addition, LFCS is a single detector measurement, which means no dichroic mirror and filters are needed and spectral cross-talk will not affect the resolvability of this technique as in the Dual-Color Cross Correlation Spectroscopy (Eigen et al., 1994, Schwille et al., 1997, Schwille et al., 2001). Because the lifetime values of molecular species are reported, LFCS is also well suited to study the energy transfer in the samples and the efficiency of energy transfer can be easily calculated from measured lifetime values of different component. In this paper, we use simulations and experiments to demonstrate that the molecular weight limit set by conventional FCS is now overcome by LFCS, and the accuracy of the analysis is significantly improved compared to FCS technique.

In another study done by Enderlein's group (Gregor et al., 2007, Enderlein et al., 2005), they developed a method to use lifetime as a filter to statistically assign each photon to one channel representing one of the two component, subsequently, construct FCS curves of individual component and analyze them to obtain the diffusion and concentration information. Their instrumentation represents a powerful example of combining lifetime and FCS analysis to use the difference in lifetime of different molecular species to separate photons. The difference between their method and our method is that in our LFCS, a global and simultaneous analysis of both diffusion based and lifetime based resolvability of species is carried out as opposed to sequentially analyzing lifetime information and then FCS. No priori knowledge about lifetime is needed, and a global curve fit is performed to find the lifetime of two components as well as the diffusion and molecular brightness. Because LFCS utilizes a global analysis algorithm, the

difference in diffusion coefficient of different species also contributes to the ability of separating and quantifying two components. When the lifetime method fails to resolve two components due to inadequate difference in lifetime values, LFCS is able to integrate the advantages of both diffusion based-FCS and lifetime to resolve a mixture more robustly, as shown in the χ^2 discussion. Furthermore, thus far, no quantitative knowledge about the limitation of resolution by combining FCS with lifetime has even been known. Here, using simulations, we present statistical analysis to show the application range of LFCS, and moreover, to present numerical results of relative error analysis of LFCS analysis, which will serve as a reference guide for experimentalists for rational experimental designs.

2.3 Theoretical Basis and Experimental Setup

Various statistical methods are developed to study the fluorescence signal to extract static and dynamic information out of the system under study. FCS and fluorescence lifetime decay are among many techniques that extract dynamic information about the system from fitting different fit functions based on different theoretical models describing dynamics processes in a system. FCS studies the temporal fluctuation of fluorescence intensity at the millisecond time scale. It provides valuable information about hydrodynamics and concentration. The fluorescence lifetime analysis studies the temporal decay of the total intensity of fluorescence at the nanosecond scale, which is another widely used technique for studying molecular interactions. in the following section, the theoretical basis of them are briefly presented, more details can be found from many excellent literatures (Lakowicz, 2006b).

2.3.1 Fluorescence Correlation Spectroscopy

The theoretical background of fluorescence correlation spectroscopy (FCS) was developed in the early 1970th by Elson and Madge adapted from the theory of dynamic light scattering (DLS) (Magde et al., 1974, Elson et al., 1974). In analogy to DLS correlations in the temporal fluctuations of a signal are analyzed. In FCS the fluorescence signal of the sample is correlated to obtain information on the processes that cause the fluctuations. To measure the fluorescence of the sample a small part of it is illuminated by a focused laser beam.

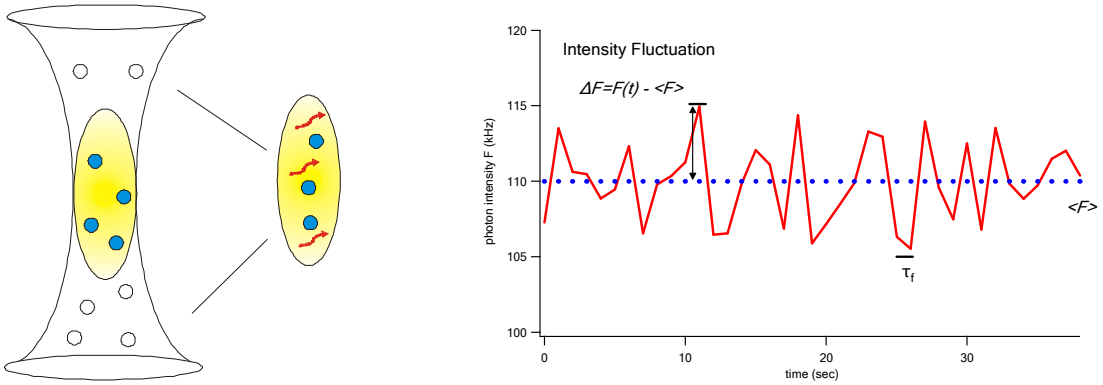

Figure 2.1: Conceptual basis of FCS. Fluorescent molecules move through an illuminated volume by diffusion or flow and cause changes of the measured fluorescence intensity (left). Typical time trace of fluorescence intensity in an FCS measurement (right).

Figure 2.1 presents the conceptual basis of FCS and shows three examples for the possible origin of fluctuations in the fluorescence signal. First, transport of fluorescent molecules through the illuminated volume can be the cause of fluctuations of fluorescence. In thermodynamic equilibrium the origin of such motion can be thermally-induced concentration fluctuations, which occur on the microscopic scale, and are known as Brownian motion. Also an external flow of the liquid transports molecules through the illuminated volume and therefore causes fluctuations in the fluorescence signal. Second, transitions between two states of different fluorescent yield can lead to fluctuations in the fluorescence if the transition occurs while the molecules traverse the excitation beam. The stability of such states and the change between different states is often

dependent on the local environment of the molecules. Therefore FCS can be used to probe the local environment of the fluorescent molecules on a microscopic scale.

FCS uses autocorrelation function to compute the fluctuation of fluorescence intensity (Elson et al., 1974, Magde et al., 1974); its main idea is to compare the intensity at time *t* with itself in the later time $t+\tau$,

$$G(\tau) = \frac{< \Delta F(t) \Delta F(t+\tau) >}{< F(t) >^2} \qquad (2.1)$$

where *F(t)* is the fluorescence intensity measured at time *t*, the angle bracket represents the time average, and $\Delta F(t) = F(t) - < F(t) >$ is the time dependent deviation of the fluorescence intensity from the average intensity (Magde et al., 1974).

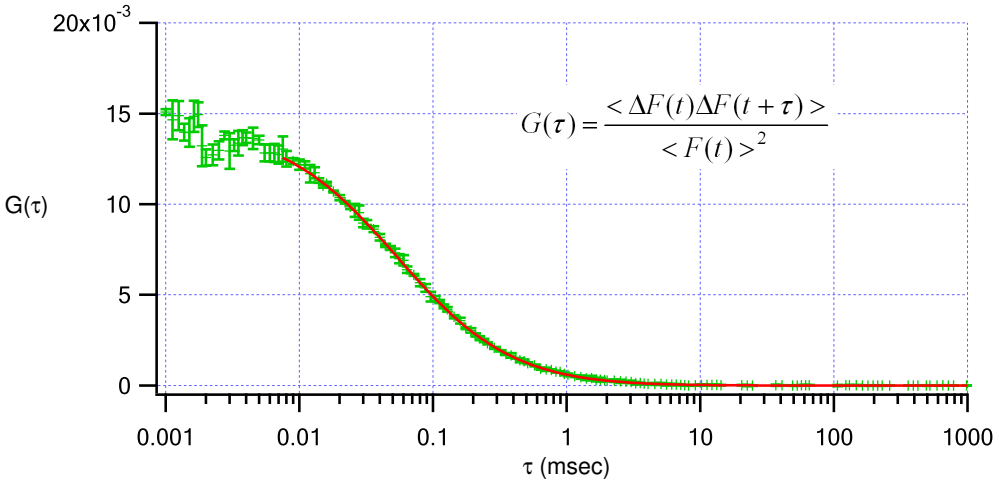

Figure 2.2 experimental data of FCS (green) and its fit curve (red).

A freely diffusing molecular species in a 3D Gaussian observation volume is described by the following equation (Krichevsky et al., 2002, Magde, 1976, Magde et al., 1974)

$$G(t) = \frac{\gamma}{CV_{3DG}}(1+\frac{8Dt}{\omega_0^2})^{-1}(1+\frac{8Dt}{z_0^2})^{-\frac{1}{2}} = \frac{\gamma}{CV_{3DG}}A(D,t)$$
$$A(D,t) = (1+\frac{8Dt}{\omega_0^2})^{-1}(1+\frac{8Dt}{z_0^2})^{-\frac{1}{2}} \quad (2.2)$$

where C is the concentration of molecules in the observation volume, $V_{3DG} = \frac{1}{8}\pi^{3/2}\omega_0^2 z_0$ is the observation volume defined by 3D Gaussian profile of the laser (Rigler et al., 2000), $\gamma = 1/2\sqrt{2}$ is the shape factor of 3D Gaussian observation volume, D is the diffusion coefficient, t is the lag time, ω_0 is the beam waist and z_0 is the axial radius of the laser beam.

In the absence of excitation saturation, the time averaged spatially dependent two-photon absorption rate by two-photon excitation is

$$W(r) = \frac{\sigma_2 I_0^2 S^2(r) f_p \alpha_p g}{2} \quad (2.3)$$

where σ_2, f_p, α_p, I_0 and g is the two-photon absorption cross section, laser pulse repetition rate, laser pulse width (full width half maximum), peak laser intensity, and a numerical factor of order unity that depends on the laser pulse temporal profile, respectively . *S(r)* specifies the spatial profile of the focused illuminating laser beam (Xu et al., 1991).

The molecular brightness of the species is defined as number of photons emitted by one fluorescent molecule in one second,

$$\Psi = k < W(0) >= \frac{\overline{F}}{N} = \frac{\overline{F}}{CV_{3DG}} \quad (2.4)$$

where k accounts for the quantum yield of the fluorophores and the detection efficiency of the instruments, and the integration is over the whole space to account for the possible excitation over all samples, $\overline{F}$ is the average fluorescence intensity measured in the detection volume and N is

the number of molecules in the observation volume of laser. The molecular brightness Ψ is a parameter that characterize the combined effect of absorption, fluorescence relaxation and detection efficiencies, thus very useful in describing fluorescent species, which will be extensively used in this thesis.

Fitting the autocorrelation function, dynamics information, such as concentration *C*, diffusion coefficient *D* of the molecular species are able to be extracted (Elson et al., 1974).

For a two-component system where two non-interacting species of distinct diffusion coefficient D are present, the FCS function is brightness-weighed sum of two components

$$G(\tau) = \frac{\gamma}{V_{3DG}} \times \frac{(C_1\Psi_1^2 A(D_1,\tau) + C_2\Psi_2^2 A(D_2,\tau)}{(C_1\Psi_1 + C_2\Psi_2)^2} \tag{2.5}$$

Since FCS is a fluctuation technique which uses relative fluctuation of intensity not absolute intensity to derive dynamic information, theoretically the autocorrelation curve for a single component system doesn't depend on the absolute steady state intensity or molecular brightness as defined in Eq. 2.4.

When two components are present, the autocorrelation is a molecular brightness weighted curve as shown in equation 2.5. The FCS function therefore shows its dependence on the molecular brightness ratio.

$$G(\tau) = \frac{\gamma}{V_{3DG}} \times \frac{(C_1 A(D_1,\tau) + C_2 S^2 A(D_2,\tau)}{(C_1 + C_2 S)^2}$$
$$S = \frac{\Psi_2}{\Psi_1} \tag{2.6}$$

As the contribution of one component to the FCS curves is dependent on the square of the brightness ratio *S*, FCS is heavily weighted by brightness ratio *S*. The implications are further studied in the chapter.

2.3.2 Rational of extending FCS technique

FCS analysis could be linked to other techniques, such as fluorescence anisotropy and fluorescence lifetime analysis through either brightness or diffusion information: translational diffusions can be associated with rotational diffusion. For example, the rotational diffusion time of a molecule, $\tau_R = \frac{4\pi R^3 \eta}{3kT}$ can be compared with the translational diffusion time $\tau_T = \frac{3\omega_0^2 \pi \eta R}{4kT}$, thus the corresponding rotational time from translational diffusion can be expressed as $\tau_R = \frac{16}{9\pi}(\frac{R}{\omega_0})^2 \tau_T$ where R is radius, ω_0 is beam radius.

This link is based on a strong assumption that the molecule is sphere in shape, otherwise, the shape factor becomes extremely complicated for the linkage between τ_T and τ_R to be used effectively. Although anisotropy report change in rotational diffusion, the simple assumption about shape makes it less convincing in studying protein-DNA interaction to link translational diffusion with rotational diffusion because proteins are often not globular.

Anisotropy, therefore, would only be useful in linking the brightness of species due to its intensity fraction rule that govern the additivity of anisotropy of different species. However, due to the many complicating issues in accurate anisotropy measurement in two photon excitation, including local motion effects, signal contamination due to scattering and autofluorecence, lifetime constrained dye choice, depolarization due to energy transfer and distortion of polarization due to high N.A lens and imperfect polarizers, we choose to combine lifetime with FCS. The same idea applies to combining lifetime with FCS. Lifetime contains no information

about diffusion, but concentration and quantum yield (molecular brightness) information is preserved, so this information could provide a link in using FCS and lifetime global fit.

2.3.3 Fluorescence Lifetime analysis

Fluorescence lifetime represents the average time an excited molecule stay in the excited state before emitting a photon, after absorbing a photon of excitation. Fluorescence lifetime is an indicator of both the intrinsic properties of the fluorophore and the environmental conditions surrounding the molecules, such as pH, ion concentration. There are well documented books and literatures discussing fluorescence lifetime (Lakowicz, 2006b, Valeur, 2002, Wang et al., 1996).

Fluorescence lifetime is sensitive to many external factors as the same as fluorescence to resonant energy transfer, collisional quenching, etc. When interpreted correctly, these induced changes in fluorescence lifetime could be applied to monitor local environment and/or interactions between host molecules and other surrounding molecules. Lifetime is less susceptible to misinterpretation due to photobleaching than intensity-based experiments such as imaging analysis. More importantly, fluorescence lifetime provides an additional contrast parameter to distinguish molecules other than spectrum.

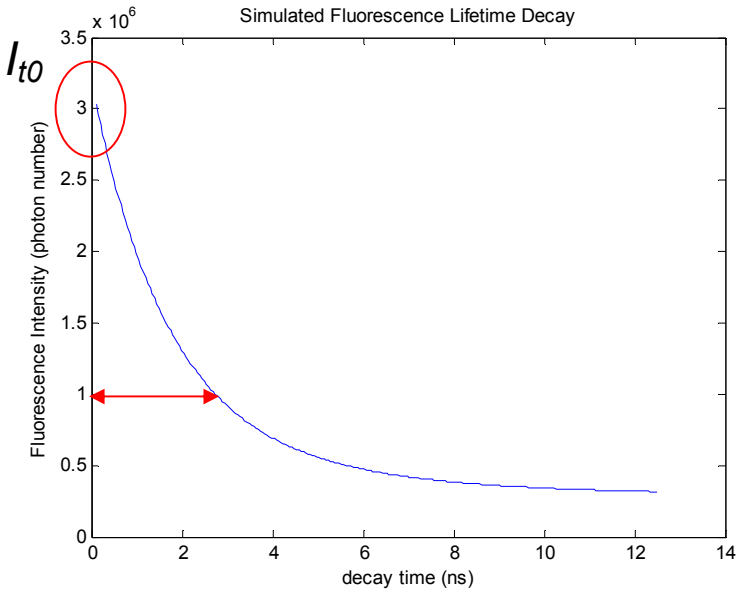

Figure 2.3: schematic of fluorescence lifetime decay, the circle denotes I_{t0} the amplitude of the lifetime decay, the red arrow denotes the average lifetime.

Fluorescence emission is a random process which means the rate of fluorescent molecules relax to ground state is proportional to the total population of molecules in the excited state, $\frac{dN}{dt} = -\frac{1}{\tau}N$ (2.7)

where N is the number of excited molecules, and τ is the fluorescence lifetime value which is typically in the nanosecond scale. The intensity of fluorescence I_t is proportional to the number of excited molecules N, $N \propto I_t$. By performing an integral of Eq. 2.7 over time, we obtain that the fluorescence of one specific type of molecule decay as an exponential function, $I_t(t) = I_{t0}e^{-\frac{t}{\tau}} + bkg$ (2.8)

where I_t is the amplitude of theoretical decay of the fluorescence, the unit is number of photons per second, bkg is the background signal.

2.3.4 Global linkage of FCS and Fluorescence Lifetime analysis

As the steady-state intensity is a time average of time-resolved decay intensity, an integration of lifetime decay over time shows the bridge between lifetime values in the lifetime analysis and molecular brightness in FCS. For a continuous exponential decay, the total fluorescence is expressed as

$$\begin{aligned} &\overline{F}T = \int_0^\infty I_t(t)dt = \int_0^\infty I_{t0}e^{-\frac{t}{\tau}}dt = I_{t0}\tau \\ &CV_{3DG}\Psi = \overline{F} \end{aligned}, \qquad (2.9)$$

Where $\overline{F}$ is the averaged steady-state fluorescence signal (count rate per second) of one fluorescent molecular species and T is the total data acquisition time of the experiment.

From eq (2.9), the amplitude of the decay is replaced as $I_{t0} = \frac{CV_{3DG}\Psi T}{\tau}$, the unit of I_{t0} is number of photons per second.

In real data acquisition, a finite time bin Δt is used to collect photons in each time bin (channel), the unit of the amplitude of the real experimental lifetime decay is number of photons per time bin Δt, $I(t) = I_t(t)\Delta t$

We therefore obtain the relationship between steady-state molecular brightness in FCS and a nano-second time scale lifetime in fluorescence lifetime measurement.

$$I(t) = \frac{CV_{3DG}\Psi T\Delta t}{\tau}e^{-\frac{t}{\tau}} + bkg \qquad (2.10)$$

For a two-component system where two fluorescent components with distinct lifetimes are present, there are generally two cases:

CASE 1: when two types of fluorophores are in the system, the quantum yield Q, therefore brightness ψ and lifetime τ of the two fluorescent species are not linearly associated,

$$\begin{aligned}\tau_1 &= \frac{1}{k_{f1}+k_{nf1}} \\ \tau_2 &= \frac{1}{k_{f2}+k_{nf2}}\end{aligned} \quad \text{and} \quad \begin{aligned}Q_1 &= \frac{k_{f1}}{k_{f1}+k_{nf1}} \\ Q_2 &= \frac{k_{f2}}{k_{f2}+k_{nf2}}\end{aligned}$$

, where k_f and k_{nf} are fluorescence rate and non-fluorescence rate of one particular species.

In this case, two species of distinct lifetime are present, the total fluorescence decay can be expressed as a sum of two component species

$$I(t) = \frac{C_1 V_{3DG} \Psi_1 T \Delta t}{\tau_1} e^{-\frac{t}{\tau_1}} + \frac{C_2 V_{3DG} \Psi_2 T \Delta t}{\tau_2} e^{-\frac{t}{\tau_2}} + bkg \tag{2.11}$$

CASE 2: in cases when there is only one fluorophore in the system that transition between two states due to quenching, the fluorescence rate k_0 of one fluorophore can be assumed to be invariant in the dynamics process, only the non-fluorescent pathways k_{nf} affect the quantum yield,

$$\begin{aligned}\tau_1 &= \frac{1}{k_0+k_{nf1}} \\ \tau_2 &= \frac{1}{k_0+k_{nf2}}\end{aligned} \quad \text{and} \quad \begin{aligned}Q_1 &= \frac{k_0}{k_0+k_{nf1}} \\ Q_2 &= \frac{k_0}{k_0+k_{nf2}}\end{aligned}$$

, assuming no absorption cross-section change, this corresponds to the results that the ratio of lifetime equals to the ratio of brightness of each species, $\frac{\Psi_2}{\Psi_1} = \frac{Q_2}{Q_1} = \frac{\tau_2}{\tau_1}$. This is a very strong constraint when implemented into eqn (2.11) which yields

$$I = \frac{\Psi_1}{\tau_1} VT\Delta t (C_1 e^{-\frac{t}{\tau_1}} + C_2 e^{-\frac{t}{\tau_2}}) + bkg \tag{2.12}$$

In sum, the total intensity in lifetime decay is expressed precisely in terms of contributions from individual component, weighted by their lifetimes. Each component's brightness is linked with their lifetime, and this relationship is reflected in each component's amplitude. This automatically decomposes the total intensity of the whole system into contributions from individual component.

2.4 Materials and Methods

2.4.1 Instrumentation

Two photon excitation was provided by a mode-locked Tsunami Ti: Sapphire laser pumped with a 532-nm 5W Millenia solid-state Nd:YVO4 laser (Spectra-Physics, Mountain View, CA). The laser is fed to a IX-71 Olympus microscope (Olympus America, Center Valley, PA) and focused into the sample with a 60 × UPLSAPO 1.2 NA water-immersion objective lens (Olympus America, Center Valley, PA). Fluorescence collected through the objective lens passed through a dichroic mirror (675 DCSX) and was collected by Hamamatsu H7422-40 PMT (Hamamatsu Photonics, Japan) using the time-correlated single-photon-counting (TCSPC) technique. The signals were processed by Picoharp 300 (Picoquant, Germany).

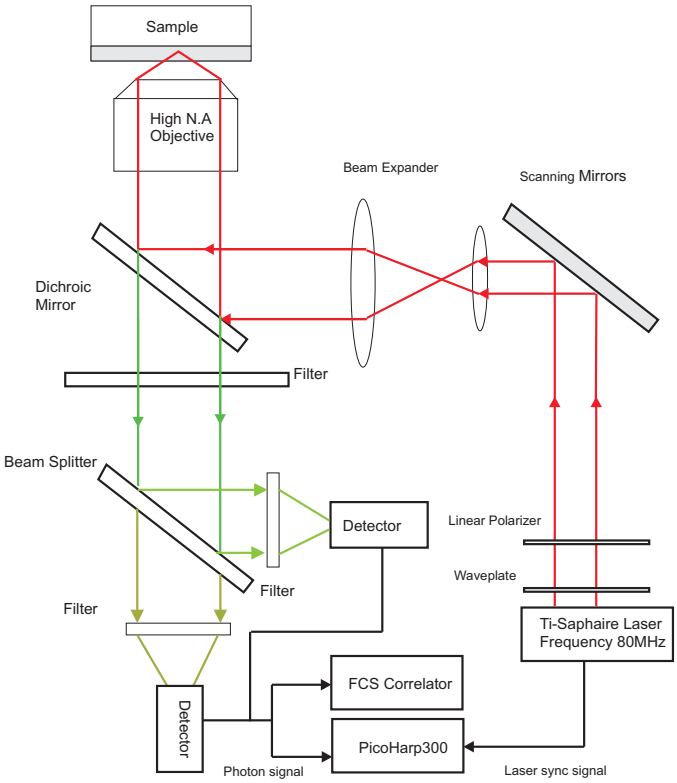

Figure 2.4: The schematic drawing of the FCS and fluorescence lifetime set up.

The experimental FCS data and fluorescence lifetime data was generated from time-tagged photons by Symphotime software (Picoquant, Germany). The FCS setup was calibrated using rhodamine 6G (R6G) solution. The laser observation volume is calibrated by fitting FCS data to a one-component free diffusion model Eq. 2.2. Based on the known diffusion coefficient of R6G, D=0.30μm^2/ms, the radial width and axial length of a 3-D Gaussian observation volume of the laser is measured to be 0.35μm and 1.75μm, respectively. The fluorescence lifetime measurement was calibrated by measuring the lifetime of R6G solution as well. Its standard lifetime 4.08ns was used as standard calibration before each experiment.

2.4.2 Sample Preparation

In the single fluorophore experiment, enhanced green fluorescent proteins eGFPs are used. They are purified using standard column chromatography procedures published elsewhere (Kelly et al., 2007).

In the binary-dye experiment, the stock solutions of Rhodamine 6G (R6G), Rhodamine B (RB) (Acros Organics, Morris Plains, NJ) were dissolved in water and were diluted to appropriate concentration for FCS and lifetime experiment before each experiment. The dyes were excited at 780nm under two photon excitation mode. For all of the mixture measurements, we recorded data for 300seconds.

2.4.3 Simulation

A simulation routine of FCS data and lifetime data similar to Meseth's (Meseth et al., 1999) is used here. Matlab codes are written to construct FCS curves and fluorescence lifetime decays according to Eqs. 2.5 and 2.11 for systems composed of two molecular species, each of which possesses distinct diffusion coefficients, molecular brightness and lifetime.

Noise was added to both fluorescence decay and FCS curves simulating the statistical fluctuations of real data. For FCS, The signal to noise ratio S/N in FCS measurement is defined (Koppel, 1974) as $\frac{S}{N} = \frac{G(t)}{Var(G(t))^{\frac{1}{2}}}$ (2.13)

The distribution of molecules in the observation volume can be described by a Poissonian distribution. In the classical paper by Meseth (Meseth et al., 1999) which aimed to understand the resolution of FCS, the variance of FCS is estimated by Koppel (Koppel, 1974),

$$Var(G(\tau)) = \frac{1}{M}\frac{1}{N^2}\{\frac{(1+g^2(\Delta\tau)(1+g^2(\tau))}{1-g^2(\Delta\tau)} + 2mg^2(\tau)\} + \frac{1}{M}\{\frac{2(1+g^2(\tau))}{N<n>} + \frac{1}{<n>^2}(1+\frac{g(\tau)}{N})\} \quad (2.14)$$

Where $\Delta\tau$ is the channel width of the correlator, $<n>$ is the average count rate per correlator channel during the measurement, $M=t/\Delta\tau$ is the number of counting intervals, t is the measuring time of the experiment, N is the average number of particles, m=τ/Δτ. $g(\tau)=(1+\frac{\tau}{\tau_D})^{-1}$ is based on autocorrelation for simple two-dimensional diffusion, τ_D is the average diffusion time of the molecule.

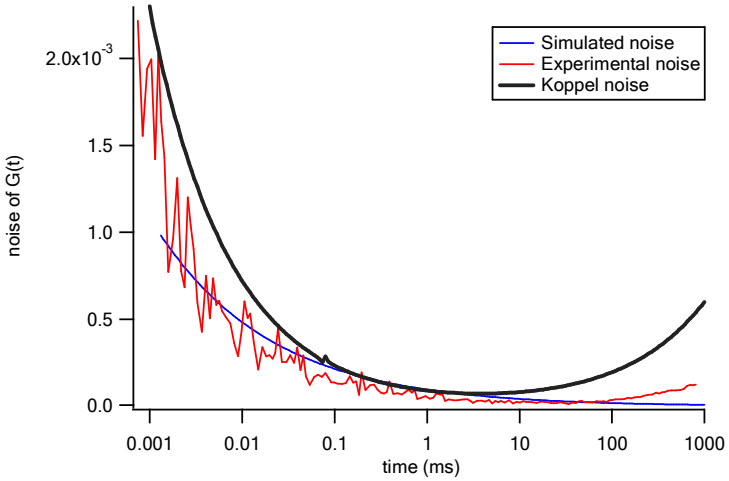

Figure 2.5: comparison of Koppel noise and our empirical noise generation.

This noise generation is not used in this paper, because the deviation from the real noise is too large at lag time longer than 1ms and the fit yielded χ^2 less than 1 indicating the noise by Koppel method is overestimated compared to real experiment as shown in figure 2.5. This is the reason I chose not to follow their suit and developed my own empirical noise simulation. Similar strategy of simulating FCS noise has also been used in (Sengupta et al., 2003). From the work of Krichevsky and Bonnet (Krichevsky et al., 2002) the amplitude of the variance of autocorrelation function is $VarG(\tau)=Var(\frac{<\delta F(t)\delta F(t+\tau)>}{<F>^2})=\frac{1}{T(\Psi N)^2}$, we arrive at

$$\sigma_{FCS}=a\sqrt{\frac{1}{T(\Psi N)^2}}\tau^b \qquad (2.15)$$

This is a qualitative measure of the noise in relation with molecular brightness, data acquisition time and number of molecules in autocorrelation function and we need to add a prefactor *a* and parameter *b* to figure out an empirical noise level for our specific setup.

Another empirical method of generating noise in FCS is proposed by Starchev (Starchev et al., 2001) in which the variance of autocorrelation function is expressed by three terms related to the number of molecules and average fluorescence intensity.

$$Var(G(\tau)) = \frac{1}{N^3}\left(\frac{a_1}{F} + \frac{a_2}{F^2}\right)\frac{1}{1 + x^2\frac{\tau}{\tau_c}} + \frac{c_1}{N^2}\frac{1}{\left(1 + x^2\frac{\tau}{\tau_c}\right)^{0.33}} \tag{2.16}$$

Where a_1, a_2 and a_3 are fitting parameters, F is the average fluorescence intensity and τ_c is the diffusion time. I didn't use this method as I found that the parameters display some instability.

Therefore, the noise of FCS was simulated using an empirical power law equation. $\sigma_{FCS}(\tau)$ is the standard deviation in FCS simulation at channel τ,

$$\sigma_{FCS}(\tau) = \frac{a}{\Psi N\sqrt{T}}\tau^b \times Gaussian(0,1) \tag{2.17}$$

where a is the pre-factor that is empirically determined to be 0.5 and b is -0.35 for our set-up, N is the number of molecules in the observation volume, Ψ is the molecular brightness of the species and T is the total data acquisition time of the experiment. $Gaussian(0,1)$ is a random number generator in Matlab which creates random number based on Gaussian distribution with mean value 0 and the variance 1.

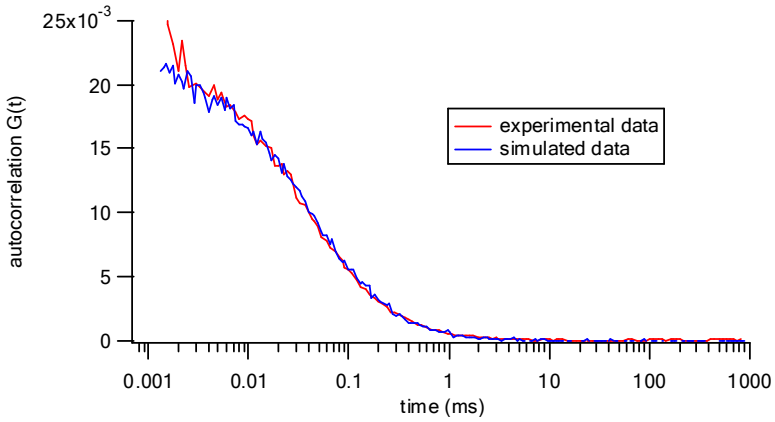

Figure 2.6: simulated autocorrelation curves for three-dimensional diffusion with a concentration of 30nM in the sample volume and a diffusion coefficient 0.3μm^2/ms. The statistical noise was simulated for t=300s measurement time with an average molecular brightness 4kHz. The real experimental data of rhodamine 6G in water with the same experimental condition is also plotted.

The noise in the fluorescence lifetime measurement obeys a Poisson distribution as it is a photon counting process. According to Poisson distribution, the variance of signal equals to the mean of the signal. $\sigma_{lifetime}(t)$ is the standard deviation in the lifetime simulation,

$$\sigma_{lifetime}(t) = \sqrt{I(t)} \tag{2.18}$$

Where *I(t)* is the fluorescence decay signal in each channel *t*. Due to the long data acquisition time (~300s), the noise of lifetime data is not visible by visual inspection, thus not shown here.

2.4.4 Data analysis

For curve fitting, an iterative global fit procedure was performed with the Levenberg-Marquardt algorithm to minimize χ^2 using Igor Pro (Wave Metrics, Lake Oswego, OR). The goodness of fit is judged by the reduced χ^2 which measures the difference between the fitted function *y* and

the simulation data y_i weighted by standard deviation σ_i and divided by total degree of freedom (n-p),

$$\chi^2_{FCS} = \frac{\sum_{i=1}^{n_1} \left(\frac{G(t_1) - G_i(t_1)}{\sigma_{FCS}(t_1)}\right)^2}{n_1 - p_1} \tag{2.19}$$

$$\chi^2_{lifetime} = \frac{\sum_{j=1}^{n_2} \left(\frac{I(t_2) - I_j(t_2)}{\sigma_{lifetime}(t_2)}\right)^2}{n_2 - p_2} \tag{2.20}$$

$$\chi^2_{LFCS} = \frac{\frac{1}{2}\frac{n_1 + n_2}{n_1}\sum_{i=1}^{n_1} \left(\frac{G(t_1) - G_i(t_1)}{\sigma_{FCS}(t_1)}\right)^2 + \frac{1}{2}\frac{n_1 + n_2}{n_2}\sum_{j=1}^{n_2} \left(\frac{I(t_2) - I_j(t_2)}{\sigma_{lifetime}(t_2)}\right)^2}{n_1 + n_2 - p_3} \tag{2.21}$$

Where n_1 and n_2 is the number of data points in autocorrelation data and fluorescence lifetime data respectively, in this paper, n_1 and n_2 are all 250.

p_1, p_2 and p_3 is the number of free parameters in the fit of FCS, lifetime and LFCS respectively.

	p_1	p_2	p_3
One-component	2	2	3
Two-component	4	3	5

t_1 and t_2 is different time scale for FCS and lifetime decay respectively. t_1 is at millisecond scale and t_2 is at nanosecond scale. The term $\frac{n_1 + n_2}{n_1}$ and $\frac{n_1 + n_2}{n_2}$ in front of the summation is to account for different lengths of data points in two methods.

The χ^2 of the global fit composed of two fit functions are average of both χ^2 square from two function individually. When one function is able to fit its data successfully reporting a small χ^2 close to one and the other function can't fit reporting a χ^2 much larger than one, the global

χ^2 square value is medium value of the two individual χ^2 (smaller than the large χ^2 of the bad fit function).

Table 2.1: the comparison of parameter setting in different fit methods

Method	Global parameters				Local parameters			
	C_1	C_2	ψ_1	S= ψ_2/ψ_1	D_1	D_2	τ_1	τ_2
1. FCS	✓	✓	×	✓	×	✓	-	-
2. FCS with intensity constraint	✓	✓	×	*a*	×	✓	-	-
3. LFCS	✓	✓	×	✓	×	✓	×	✓
4. LFCS, free ψ1	✓	✓	✓	✓	×	✓	×	✓
5. LFCS with brightness and lifetime linkage	✓	✓	×	*b*	×	✓	✓	✓
6. LFCS with brightness and lifetime linkage, free ψ1	✓	✓	✓	*b*	×	✓	✓	✓

✓ is fitting parameter, × is fixed parameter

a is $\Psi_2 = (\frac{F}{V} - C_1\Psi_1)/C_2$

b is $\frac{\Psi_2}{\Psi_1} = \frac{\tau_2}{\tau_1}$

Table 2.1 is a compilation of the parameter setting of all the analysis method in this paper. ✓ and × are to indicate which parameters are set to be fitting parameters and which are fixed during curve-fitting.

2.4.5 Correction of Instrument Response Function (IRF) impact in lifetime analysis

In fluorescence lifetime analysis, the uncertainty in measuring the onset of laser pulses is described as instrument response function. We used a tail-fit method to analyze the fluorescence lifetime data to avoid this impact. In other words, the decay data excluding the rising part - a tail region of lifetime decay data is chosen and analyzed. Analytical analysis and computation show that when the lifetime is 1.5 times larger than the full width at half maximum (FWHM) of system IRF, reasonable fluorescence lifetimes can be obtained by fitting the decay tail without taking into account IRF (Ma et al., 2005). This gives a guidance of system precision limit for fluorescence lifetime analysis by tail fitting.

However, the exclusion of IRF from the analysis will decrease the total collected photons from the experiments, thus alter the molecular brightness of the molecules. Based on the idea that the amplitude of the decay contains the concentration and molecular brightness information, the minimal intensity affected by the Instrument Response Function (IRF) region in the lifetime decay needs to be accounted for in the calculation of total intensity.

We use a pre-factor α to denote the ratio of intensity in the tail-fit region and total intensity including IRF.

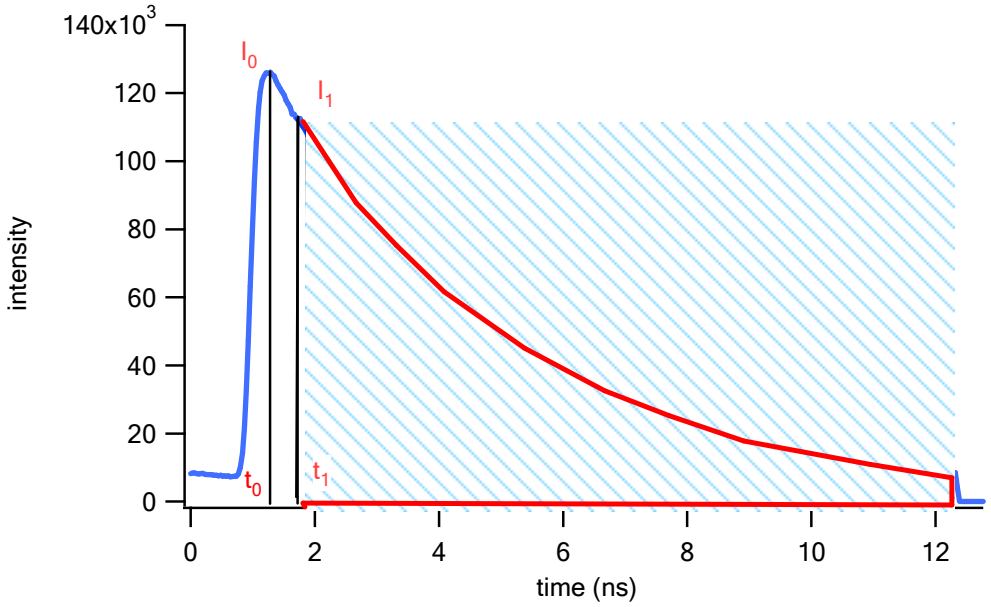

Figure 2.7: the tail-fit scheme in the experimental fluorescence lifetime analysis. The blue curve is the experimental data and the red curve is the fit of the tail region of the data.

This factor α could be pre-measured from stock solution. For example of R6G, $\alpha_1 = \frac{I_1 \tau}{FT\Delta t}$ =0.81, this fraction parameter is to account for the minimal intensity fraction of instrument response function (IRF) in the total intensity. For unknown dyes, the faction α_2 could be estimated from comparison with fraction of known dyes's α_1 , $\alpha_2 = \frac{\alpha_1 \tau_2 e^{-\frac{t_1 - t_0}{\tau_2}}}{\alpha_1(\tau_2 - \tau_1) + e^{-\frac{t_1 - t_0}{\tau_1}} \tau_1}$. Otherwise, the introduction of IRF into the analysis would cause 1) additional parameter to account for the shift in IRF of different species due to different emission. 2) the failure to determine the absolute amplitude information in fluorescence lifetime decay for different species.

2.5 Results and Discussion

In FCS, the ability to resolve multiple molecular species in a mixture is achieved from the substantial difference in the diffusion coefficients among species. When two species have at least 2.5 fold different diffusion coefficients, the minor component species whose concentration is 10% of the major component, is possible to be resolved (Meseth et al., 1999). In this new proposed method, LFCS incorporates additional information from fluorescence lifetime into fluctuation-based spectroscopy FCS to perform a global analysis, which dramatically increases the resolution of multi-component system.

Two types of systems were examined, 1) simulation data of two-component system was analyzed to show the possibility of the technique to resolve multi-component when the two component

share similar diffusion properties, furthermore, the enhanced accuracy of the technique was studied through simulations, 2) experimental data of binary-dye mixture was analyzed to verify the method's capability of resolving two molecular species with the same diffusion coefficient.

The simulation procedure used in this paper provides a convenient assessment of the application range of the new LFCS method because it is not practical to employ thousands of different fluorophores with different diffusion, lifetime and brightness values to test the feasibility of LFCS.

2.5.1 Resolvability analysis

We firstly want to understand under what condition LFCS is able to detect the presence of two species in a system. This knowledge will serve as a practical guide for any future experimental study aiming at resolving multiple species.

To do this, the theoretical FCS and fluorescence decay data of two-component mixtures were simulated according to the Method part. The simulation data was then fit by a single-component LFCS, FCS and lifetime model, respectively. It is expected that a fit of the two-component system by a single-species model will result in a misfit. The reduced χ^2 from this misfit is a convenient measure of the systematic deviation induced by forced fit to a single-species model. A reduced χ^2 value of one indicates that the model is correct in describing the data; whereas χ^2 greater than one indicates that the one-component model is wrong and more than two species is present.

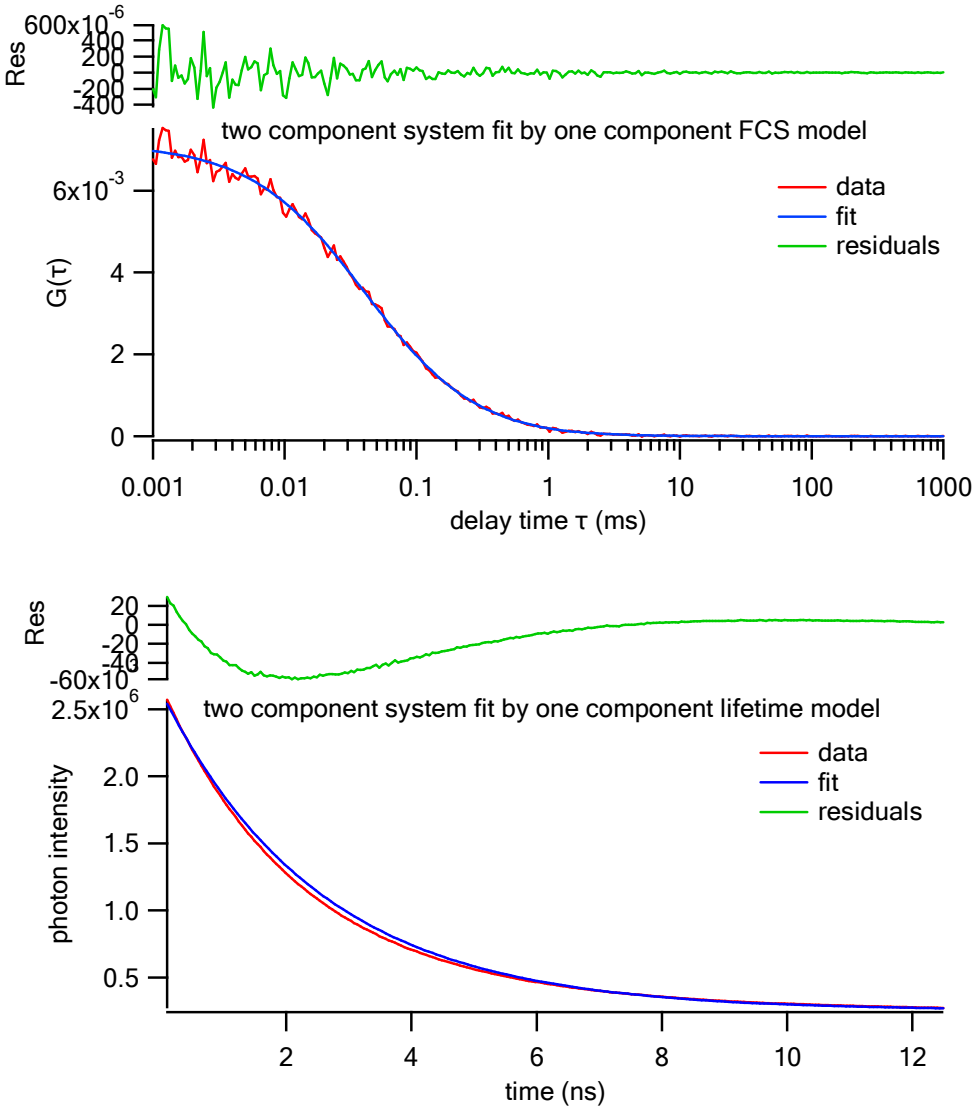

Figure 2.8: The simulation data of two-component system was fit by one-component FCS and one-component lifetime. C_1=300nM, C_2=240nM, D_1=0.3μm^2/ms, D_2=0.3μm^2/ms, τ_1=4ns, τ_2=2ns, Ψ_1=5kcpsm, Ψ_2 =10kcpsm. The fit by LFCS is indistinguishable from individual FCS and lifetime fit, thus not shown.

	FCS fit	Lifetime fit	LFCS fit
χ^2	1.1	1094.4	551.2

It is clear that because the two components possess the same diffusion property, the FCS reports a χ^2 close to 1, thus fails to recover the two components based on reduced χ^2, but the lifetime fit report the presence of two components due to the difference in their lifetime values and reported a much bigger χ^2. Similarly, when the lifetimes of two components are close, the difference in the diffusion coefficient of two components differentiates two species as well.

To study the dependence of the LFCS resolvability on lifetimes and diffusion coefficients, we kept the concentrations and brightnesses of two species constant, but varied the diffusion coefficient and lifetime of minor component systematically while maintaining that of the major components constant. The results are best represented in the form of a contour plot of χ^2 as a function of the ratio of both lifetime and diffusion coefficient.

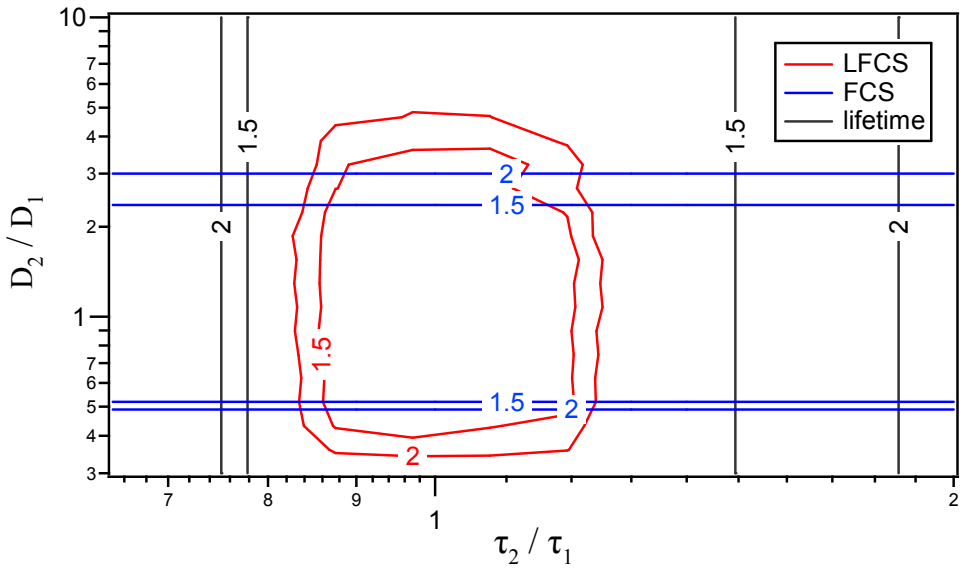

Figure 2.9: The comparison between contour plots of reduced χ^2 fit by one component FCS, lifetime and LFCS model, respectively. Simulations of two component system are constructed at varying diffusion coefficient and lifetime ratio. In the simulation, the minor component's concentration C_2 is 30nM, 10% of the major component C_1=300nM. Other simulation parameters

Ψ_1=10 kcpsm, Ψ_2=20 kcpsm, D_1=0.03um2/ms, τ_1=4ns, τ_2=2.6ns – 8ns. The minimal value of χ^2 occurs at the lifetime ratio of 1 and diffusion coefficient ratio of 1. The χ^2 was calculated for data acquisition time 300s.

The red curves in Figure 2.9 show the reduced χ^2 contour plot of a two-component system fitted by one-component LFCS model. When χ^2 is near 1, the signal statistics are not good enough to detect the presence of two species. It is clear that the deviation from single-component model is minimal when the two species are of the same diffusion coefficient and lifetime value. An increase of χ^2 appears from the center of figure 2.9 when the ratios of diffusion coefficient and lifetime are changed away from 1. In the area where χ^2 >1, it indicates that the one-component model is not adequate to describe the system which means that in this case, LFCS is able to report the presence of two species.

The same two-component simulation data was also fit by one-component standard FCS and one-component standard lifetime model. Due to the fact that the standard FCS only uses diffusion coefficient to distinguish different species, the standard FCS gives invariant resolvability at different lifetime ratio, therefore, the χ^2 of one-component FCS fit displays a horizontal line pattern. Similarly, the χ^2 of one-component fluorescence lifetime analysis displays a perpendicular line pattern for its independence on diffusion coefficients of species. From figure 2.9, FCS analysis shows better sensitivity at detecting two components than LFCS. This is due to the nature of global analysis that the χ^2 is an average of two different fits. The global χ^2 will result in a smaller χ^2 when lifetime analysis is unable to fit yielding a χ^2 close to one of lifetime and reduce average global χ^2 of the FCS and lifetime.

In the lifetime analysis, LFCS shows superior sensitivity than standard lifetime analysis. This is caused by the incorporation of intensity information into the lifetime analysis. Conventional

fluorescence lifetime is irrelevant to the intensity, but in LFCS its amplitude of fluorescence lifetime decay is directly linked to the measured average photon intensity in the experiment. Therefore additional constraint of intensity is added into the LFCS resolvability analysis, hence global LFCS shows superior sensitivity than lifetime analysis alone.

The results of FCS fit match with Meseth's results (Meseth et al., 1999) meaning our simulation procedure is correct. It is clear in figure 2.9 that the LFCS is able to detect a greater area in the two dimensional space composed of ratios of lifetime and diffusion coefficient. In figure 2.9, FCS technique is able to detect the presence of second component when the diffusion coefficient ratio is less than 0.5 or larger than 2.5, on the other hand, lifetime technique is able to resolve two components when the lifetime ratio is less than 0.78 or larger than 1.5, but LFCS is able to resolve more combination of D and τ in this two dimensional space.

For instance, when lifetime ratio is less than 0.78, no fluorescence lifetime information can be obtained, but LFCS can resolve the lifetime because the global fitting of LFCS utilize the different diffusion coefficients of the two components to separate species. While FCS and lifetime analysis only obtain either diffusion coefficient or lifetime value respectively, LFCS is able to simultaneously obtain information of both diffusion and lifetime properties.

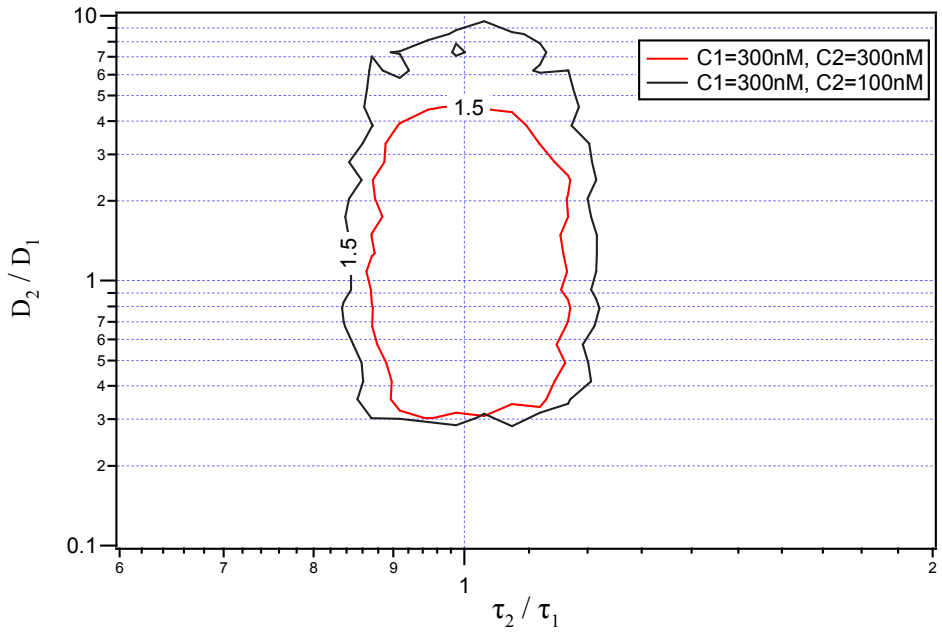

Sample	C_1(nM)	C_2(nM)	D_1(μm^2/ms)	D_2(μm^2/ms)	Ψ_1(cpsm)	Ψ_2(cpsm)	τ_1(ns)	τ_2(ns)
1	300	300	0.03	variable	5	5	4	variable
2	300	100	0.03	variable	5	5	4	variable

Figure 2.10: The comparison of χ^2 when the minor component's concentration C_2 is 33% and 100% of that of the major component C_1. The parameters' values are shown in the table above.

As the minor component contribute less (such as less concentration) to the whole system, shown in figure 2.10, in order to differentiate the two components, the difference in their diffusion or lifetime need to grow bigger as indicated by a larger area in the χ^2 plot meaning more space in the two dimensional are unable to be resolved. As in Eq. 2.15, the noise of FCS is reversely proportional to the molecular brightness, therefore when the absolute brightness of each species is decreased, the resolvability of the technique would be worse.

Overall, this χ^2 plot demonstrates the advancement of LFCS over conventional FCS and FLIM that the presence of two-component is more sensitively detected by LFCS. This plot can serve as

a practical guide for applications of LFCS, which indicates when and where this method is powerful than others.

2.5.2 Simulation results of two-component system

The study on the reduced χ^2 is aimed to understand under what experimental condition, additional species is clearly resolvable by curve fitting. The next step is to determine how accurately this new LFCS method is able to determine multi-component's concentration and other dynamics information such as diffusion and lifetime properties.

In order to investigate whether LFCS remains highly accurate in resolving a mixture of two-components over a wide range of concentrations, we simulated a series of two-component mixture according to Eq. 2.5 and 2.11. In this simulation, the concentration of major component C_1 is maintained as a constant at 300nM, and the minor component's concentration C_2 is diluted by half each time from 80% down to 10% of the major component's. The molecular brightness of the major component Ψ_1 is twice of that of the minor component Ψ_2. The simulated data was then fit by two-component LFCS model in an attempt to resolve the mixture.

When the brightness ratio S is unknown in a two component FCS fit, huge error bars of concentration of each component will appear. In other words, when the brightness ratio between two components is not known, FCS is unable to recover two components correctly. When an assumption is made about the brightness ratio S either by rough estimation from independent measurements from other techniques or arbitrary guesses, the error of recovered concentration decrease but the absolute values of the concentration are problematic depending on the assumed molecular brightness ratio. The results are plotted in figure 2.11.

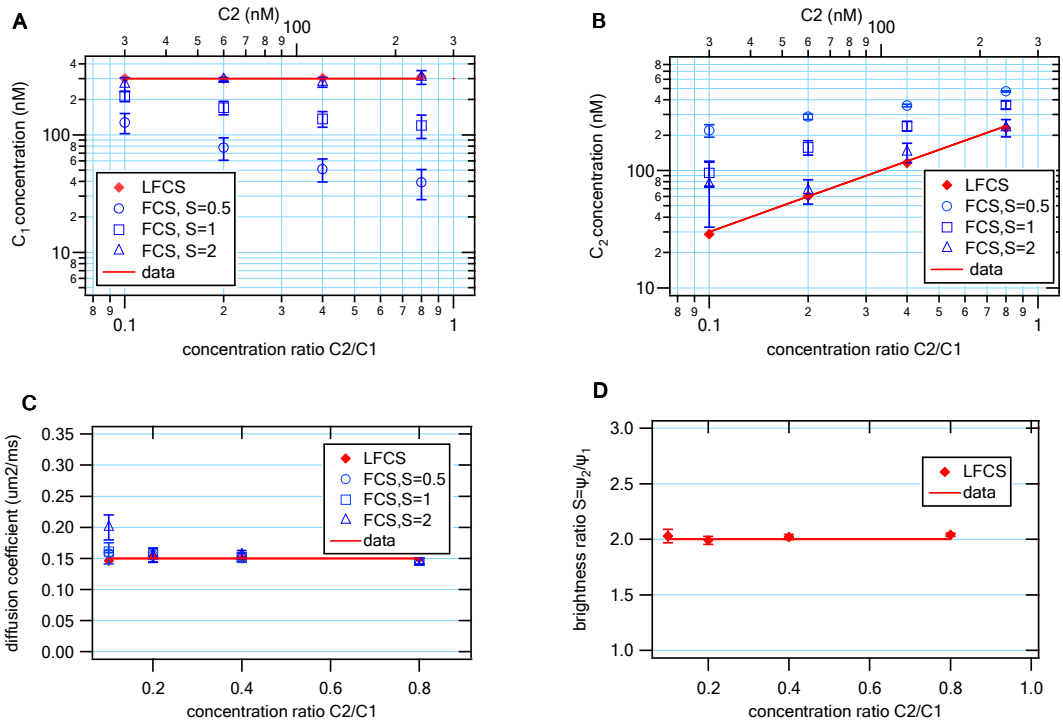

Figure 2.11: Two component LFCS fit of simulation data of a series of titration of two-component system. In the simulation, major component's concentration C_1 is kept at 300nM, minor component C_2 is decreased from 240nM to 30nM, brightness Ψ_1=10cpsm, brightness ratio $S = \psi_2/\psi_1$=2, lifetime τ_1=4ns, τ_2=3ns diffusion coefficient D_1=0.3um2/ms, D_2=0.15um2/ms. In the LFCS fit, D_1, ψ_1, τ_1 are kept as fixed parameter in the analysis, the other parameters are fitting coefficients. (A) the recovered concentration of C_1. (B) the recovered concentration of C_2. (C) the recovered diffusion coefficient D_2. (D) the recovered brightness ratio S.

C_1(nM)	C_2(nM)	D_1(μm^2/ms)	D_2(μm^2/ms)	Ψ_1(cpsm)	Ψ_2(cpsm)	τ_1(ns)	τ_2(ns)
300	variable	0.3	0.15	10	20	4	2

By providing a guessed brightness ratio, the FCS fits are stable and provide the recovered concentrations of two components with a reasonable standard deviation, but it is also clear that only when the brightness ratio is guessed correctly at S=2 which is the input simulation ratio, the resulting concentrations are accurately consistent with input concentration values.

Given the different guess of brightness ratio, the recovered concentration could lead to erroneous judgment about the composition of the system. This highlights the importance of correct and accurate determination of brightness ratio S between two species.

In contrast, the results by LFCS fit show that the recovered concentration, lifetime and diffusion coefficient are very well consistent with the input simulation parameters. The errors are significantly reduced and the recovered lifetime and brightness of the two components is constant over the dilution process meaning they are concentration-independent as expected.

Another method of improving the multi-component FCS analysis is to add fluorescence intensity as a constraint. In the past, not much attention has been paid to the absolute intensity in FCS measurement owing to the fact that FCS is based on fluctuations of intensity rather than the absolute intensity itself. However, the total fluorescence intensity contains important information about molecular brightness, therefore when incorporated into multi-component FCS, can be advantageous. In order to probe the effect of incorporating average intensity into multi component FCS analysis, a set of simulations is done to a dilution process in which the minor component's concentration is decreased gradually. The fit results by both LFCS and this intensity constrained FCS analysis are shown.

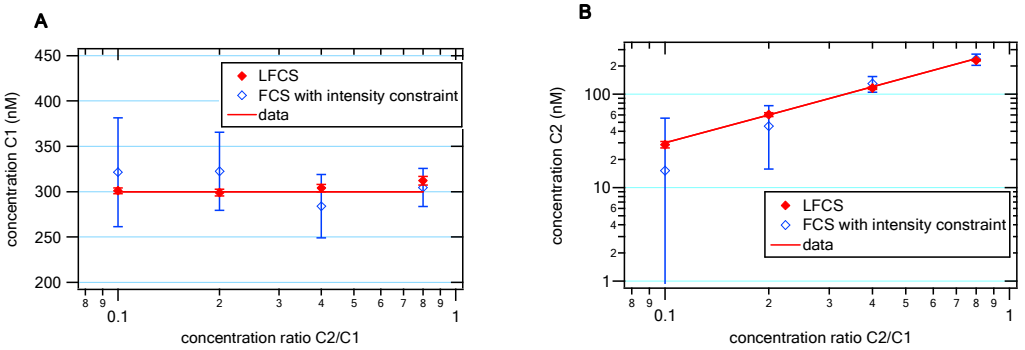

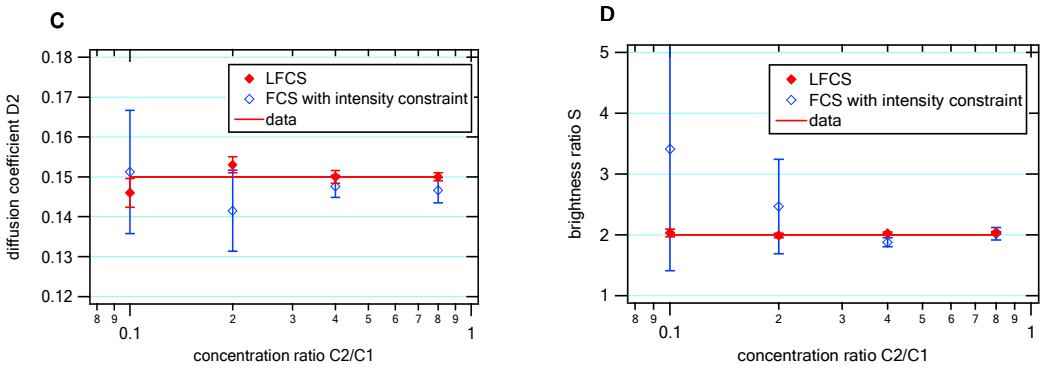

Figure 2.12: Comparison of two-component FCS with intensity constraint and two-component LFCS analysis. The data is from simulations of two-component system. C_1=300nM, C_2 decrease from 240nM to 30nM. D_1=0.3μm^2/ms, D_2=0.15μm^2/ms, τ_1=4ns, τ_2=3ns, Ψ_1=10kcpsm, Ψ_2=20kcpsm. (A) the recovered concentration of C_1. (B) the recovered concentration of C_2. (C) the recovered diffusion coefficient D_2. (D) the recovered brightness ratio S.

Compared to the standard FCS fit without intensity constraint, the additional constraint of total intensity provides increased accuracy at recovering the correct concentrations of both components, the diffusion coefficients and their brightness ratio. For concentration ratio >40%, the relative errors of the fit parameters are within reasonable range, but as the concentration of minor component decreases, the ability of recovering the correct concentration worsens. In comparison, the LFCS is an even stronger constraint, which is able to recover correct concentration, diffusion and brightness ratio within a broad range, and with a much smaller error.

2.5.3 Experimental results

To experimentally verify the principle of LFCS is correct for a one-component system. We used single dye system to test. Green fluorescent protein eGFP samples were measured and analyzed by one component FCS, lifetime and LFCS method.

Table 2.2: eGFP samples measured by three different methods

	C (nM)	D (μm^2/ms)	τ (ns)	χ^2
FCS	315±6	0.067±0.003	NA	0.93
Lifetime	NA	NA	2.81±0.02	1.21
LFCS	318±5	0.066±0.002	2.80±0.01	0.95

LFCS results were statistically indistinguishable from FCS and lifetime analysis. It can be understood from the fact that the one-component FCS is sufficient to recover two parameters: concentration and diffusion coefficient. Similarly, the one-component lifetime fit is sufficient to recover lifetime τ from single component system. Given that the correctness of LFCS to quantify one component systems is proven, we further study the ability of LFCS to resolve two components in a mixture experimentally.

We choose Rhodamine 6G and Rhodamine B as a binary system, because they possess the same diffusion coefficients, thus it is not possible to resolve these two molecules based on FCS analysis (Meseth et al., 1999).

To demonstrate the advantages of LFCS over FCS, a serial of dilution of rhodamine 6G and rhodamine B is analyzed. In this experiment, R6G and RB are mixed at initial concentration of [RB] =45nM, [R6G] =120nM.

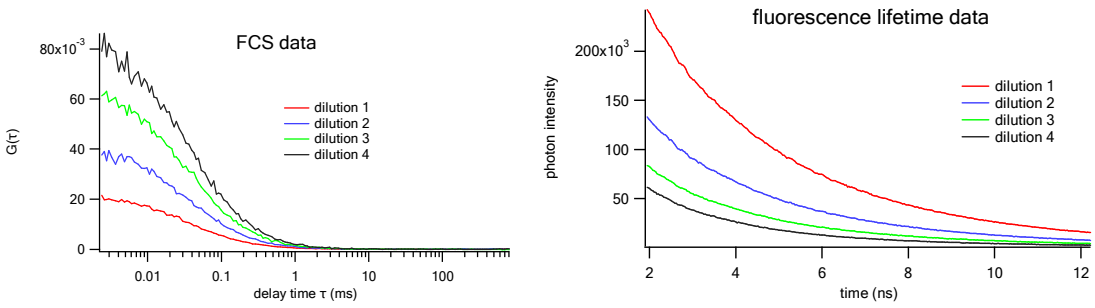

Figure 2.13: The experimental data of FCS and lifetime experiments from the four time dilution. The dilution 1-4 represents the four time dilution when the concentration of R6G is diluted from 120nM to 15nM, and the concentration of RB is maintained constant at 45nM.

Two-component LFCS was then used to analyze the data. The results from LFCS analysis is shown below.

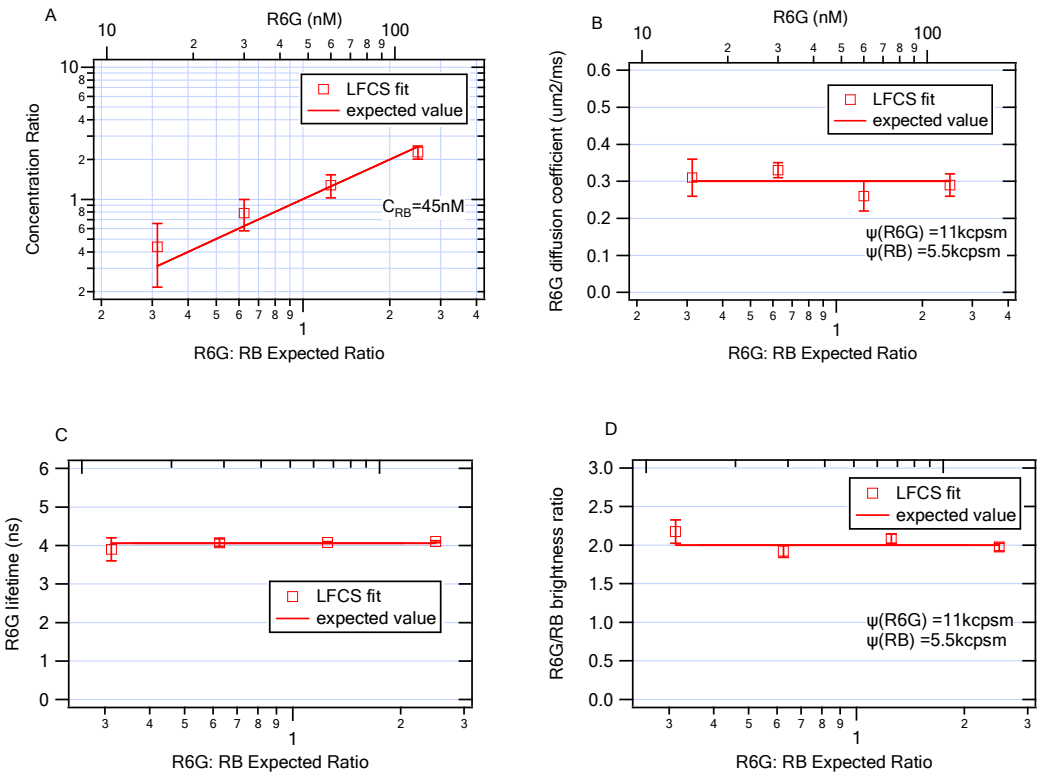

Figure 2.14. Titration experiment on mixture of rhodamine 6G and rhodamine B. concentration of rhodamine 6G is changed from 120nM to 15nM, and concentration of rhodamine B is maintained at 45nM. Ψ(R6G)=11kcpsm, Ψ(RB)=5.5kcpsm, τ(R6G)=4.1ns, τ(RB)=1.6ns, D(R6G)=0.3μm^2/ms, D(RB)=0.3μm^2/ms. (A) the recovered experimental concentration ratio of two component mixtures of rhodamine 6G and rhodamine B from two component LFCS fit. FCS results are not shown because the errors are too huge to display. (B) the recovered diffusion

coefficient of R6G by LFCS (C) the recovered lifetime of R6G by LFCS (D) the recovered brightness ratio between R6G and RB by LFCS.

C(RB) (nM)	C(R6G) (nM)	D(RB) (μm^2/ms)	D(R6G) (μm^2/ms)	Ψ(RB) (cpsm)	Ψ(R6G) (cpsm)	τ(RB) (ns)	τ(R6G) (ns)
45	15-120	0.3	0.3	5.5	11	1.6	4.1

To investigate the range of LFCS resolvability, after initial measurement of the binary dye mixture, the sample is diluted with stock rhodamine B solution and remeasured, and so forth for several time. Therefore, the concentration of rhodamine 6G is reduced by a factor of two in each step, but the concentration of rhodamine B is maintained constant.

The concentration ratio measured by two-component LFCS from each measurement is plotted in Figure 2.14A. The recovered value is in excellent agreement with the expected dilution ratio. The dilution factor of 2 is clearly indicated as a linear slope in the log-log plot in figure 2.14A. The error bars for each data point is one standard deviation of that parameter. The molecular brightness, the lifetime and the diffusion coefficient of R6G are in good agreement with independent measurement of stock solution of R6G, shown in figure 2.14B, C and D.

In summary, the fitted rhodamine 6G diffusion coefficient, lifetime and brightness ratio shown in figure 2.14 indicates that LFCS can successfully resolve the two species across a broad range of concentration ratio, and this resolution is not achievable in FCS due to the same diffusion coefficient of R6G and RB.

An important note is that in the LFCS fit, the diffusion coefficient, lifetime and molecular brightness of RB is measured beforehand independently from stock solution, therefore in the

LFCS analysis, five unknown fitting parameters are recovered as in figure 2.14. When the diffusion coefficient, lifetime and molecular brightness of RB is set to be free fit parameters, the fit is unstable, similar to what is reported before (Meseth et al., 1999) where diffusion coefficient of both components are required to be known to experimentally separate the two species and obtain correct concentration information. Our requirement is less stringent and doesn't disqualify the usefulness of LFCS because in most binding assays, prior knowledge of unbound species such as labeled oligos or peptides is often known from independent measurements.

Thus far, in the simulations and experiments, the molecular brightness of two species is intentionally chosen to be different to highlight the ability of LFCS to recover this brightness change. In order to demonstrate that LFCS's is able to resolve multi-species even when the molecular brightness of each species is identical, a serial of rhodamine 6G (R6G) and rhodamine B (RB) mixture is measured under 822nm excitation when the two dyes share the same molecular brightness. Similar to the previous experiment, an initial mixture of R6G and RB is measured then the RB solution is diluted while the R6G concentration is maintained constant in the mixture.

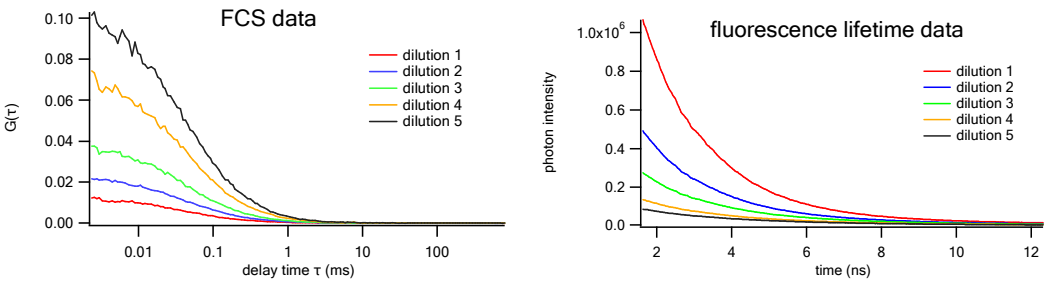

Figure 2.15: The experimental data of FCS and lifetime experiments from the five time dilution. The dilution 1-5 represents the four time dilution when the concentration of RB is diluted from 225nM to 14nM, and the concentration of R6G is maintained constant at 30nM.

Two-component LFCS was then used to analyze the data. The results from LFCS analysis is shown below.

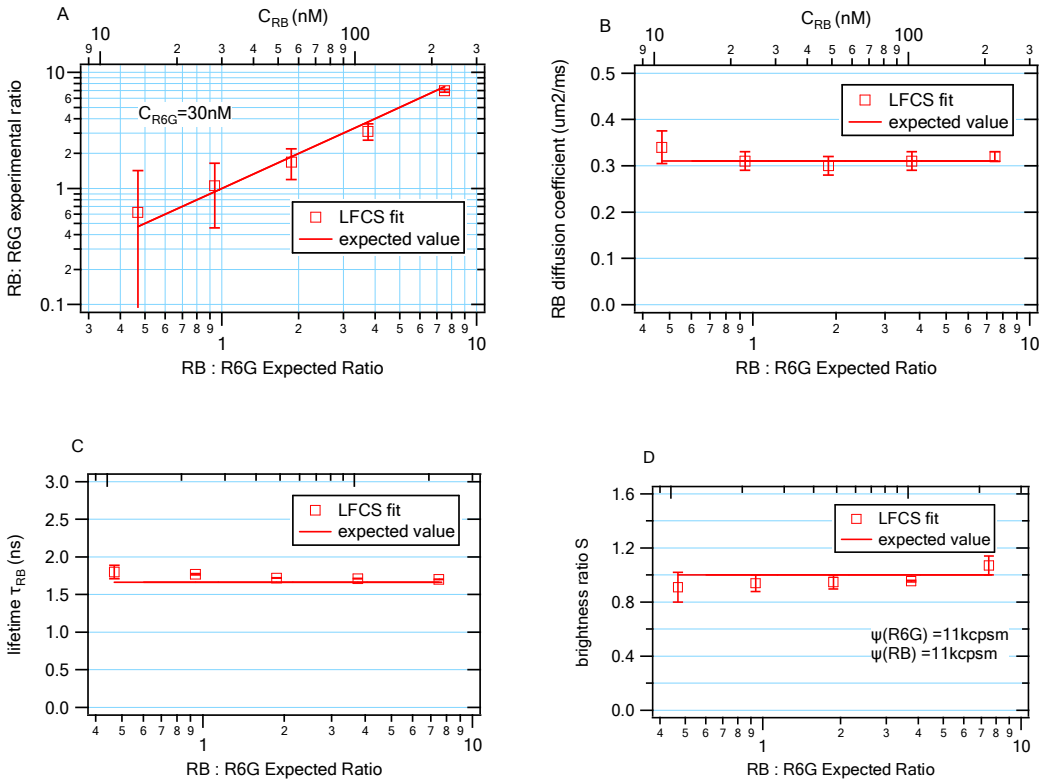

Figure 2.16. Titration experiment on mixture of rhodamine 6G and rhodamine B. concentration of rhodamine B is changed from 225nM to 14nM, and concentration of rhodamine 6G is maintained at 30nM. Ψ(R6G)=11kcpsm, Ψ(RB)=11kcpsm, τ(R6G)=4.1ns, τ(RB)=1.6ns, D(R6G)=0.3μm^2/ms, D(RB)=0.3μm^2/ms. (A) the recovered experimental concentration ratio of two component mixtures of rhodamine 6G and rhodamine B from two component LFCS fit. FCS results are not shown because the errors are too huge to display. (B) the recovered diffusion coefficient of RB by LFCS (C) the recovered lifetime of RB by LFCS (D) the recovered brightness ratio between RB and R6G by LFCS.

C(R6G) (nM)	C(RB) (nM)	D(RB) (μm^2/ms)	D(R6G) (μm^2/ms)	Ψ(RB) (cpsm)	Ψ(B6G) (cpsm)	τ(RB) (ns)	τ(R6G) (ns)
14-225	30	0.3	0.3	11	11	1.6	4.1

It is clearly shown that even when the molecular brightness of two species in a mixture is identical, LFCS is able to resolve them based on the difference in their lifetime values. This is an advantage when compared to Time-integrated Fluorescence Cumulant Analysis (TIFCA) method, which can't resolve two components when their diffusion and brightness properties are closely similar. The accuracy of LFCS is further discussed in the following section.

2.5.4 Discussion

In this work, we demonstrated that combining FCS and lifetime with global fitting can substantially increase the resolvability of multi-component and provide accurate determination of concentration, diffusion coefficient, lifetime and brightness of individual species.

Discussion of the Simulation

In the published applications of fluorescence lifetime analysis, no quantitative results have been provided regarding how the difference in lifetime values of component species affects the resolvability, moreover, no quantitative measure of accuracy of parameters recovered from data fitting are discussed. In the following section, we discuss quantitatively the impact of diffusion coefficient ratio, lifetime ratio and brightness ratio on the resolution of LFCS. The discussion of relative error of this technique presented here allows experimentalists to predict whether species can be resolved based on measured properties of fluorophores.

2.5.4.1 Influence of the diffusion ratio and lifetime ratio

In order to understand the influence of different combination of lifetime and diffusion coefficient, the relative errors of recovered parameters are used as an indicator of the accuracy. The relative error of a parameter is defined as the ratio of standard deviation of fit parameter over the absolute value of that parameter. $\delta p = \frac{\Delta p}{p} = \frac{\sqrt{Var(p)}}{p}$, where p is the input value of the simulation parameter and $Var(p)$ is the variance of the parameters from curve fitting. This is a proper quantitative measure of accuracy for parameters that have different magnitude. In the case of FCS and lifetime analysis, individual parameters including concentration, diffusion coefficient and brightness are all different in terms of unit and magnitude, hence well suited to be characterized by the relative error δp concept.

Two-component autocorrelation and fluorescence lifetime data were simulated according to Eqs. 2.5 and 2.11. In the simulation, the concentration of each component were fixed, but the minor component's lifetime τ_2 and diffusion coefficient D_2 were varied systematically while maintaining the major component's lifetime τ_1 and diffusion coefficient constant D_1, which means the ratio of lifetime and diffusion coefficient were varied. The two-component LFCS model was then applied to fit the simulation data.

The relative errors of parameters are averaged over 10 runs and mean values are plotted in figure 2.17.

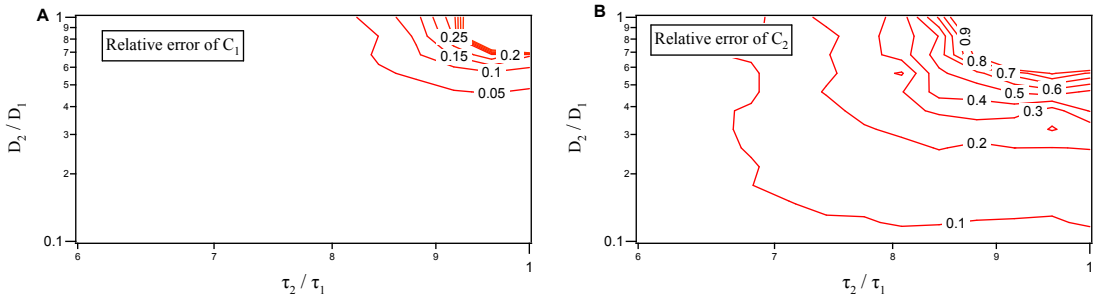

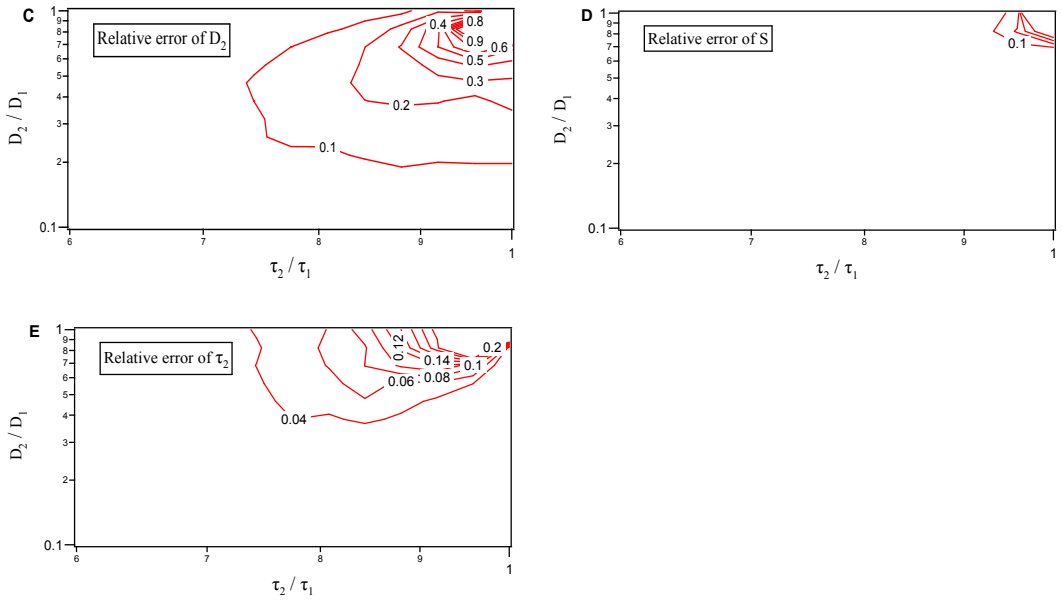

Figure 2.17: The impact of diffusion coefficient and fluorescence lifetime on the resolvability of LFCS. C_1=300nM, C_2=30nM, Ψ_1=5kcpsm, Ψ_2=5kcpsm, D_1=0.03um^2/ms, D_2=0.003-0.03um^2/ms, τ_1=4ns, τ_2=2.4ns-4ns. (A). the relative errors of recovered concentration of major component C_1. (B). the relative errors of recovered concentration of major component C_2. (C). the relative error of diffusion coefficient of the minor component D_2. (D). The relative error of brightness ratio of the minor component over major component S. (E). The relative error of lifetime of the minor component τ_2.

The contour plot shows the relative error of fit parameters, including the concentration of each component, the diffusion coefficient and lifetime of the minor component, and the brightness ratio between the minor and the major component. In this simulation, the concentration of the minor component 30nM is 10% of the major component 300nM. It is shown in figure 2.17 that the relative errors increase as the lifetime and diffusion coefficient ratio approach one due to the decrease in the distinctions between two components. This is understandable since the resolution in LFCS is achieved from differentiating the diffusion coefficient and lifetime values of different species. As shown in figure 2.17, the LFCS method is accurate at recovering fit parameter with

less than 10% relative error as long as the lifetime ratio between the two components is less than 70%.

This type of plots can serve as guide references to choose the suitable fluorophores and design rational experiments. For instance, if the diffusion coefficients of two components are the same, the lifetime ratio needs to be less than 70% in order to determine the concentration ratio with less than 10% error. If the lifetime ratio is 80%, then from the figure, we can obtain the theoretical accuracy limit of our recovered concentration ratio to be approximately 30% if the diffusion coefficient ratio is 0.5. The relative errors of the other fit parameters like brightness ratio, the lifetime and diffusion coefficient of the minor component can also be found from figure 2.17 C, D and E.

2.5.4.2 Influence of the brightness ratio S, Ψ_2/Ψ_1

Due to the quadratic dependence on brightness ratio S in FCS and linear dependence on S in the fluorescence lifetime technique, an accurate determination of S is required for correct interpretation of concentrations of component species from FCS and lifetime method. In FCS, the measurement of brightness within multiple species system has been difficult. In published literatures (Meseth et al., 1999), the brightness ratio was either independently measured or assumed to be a constant that could be pre-determined. This is rarely possible when applied in protein-nucleic acid binding and protein-protein interactions' studies. Furthermore, when multiple binding sites of biomolcules or dynamics quenching are present, the molecular brightness is a variable depending on the binding site occupation, hence a constant brightness ratio S can't be guessed or pre-measured. This problem is solved in LFCS through the combination of FCS and fluorescence lifetime analysis which provides robust resolution on the brightness ratio. In this paper, brightness ratio S is a free fit parameter that is able to be more robustly determined

compared with conventional FCS techniques, demonstrated below. This brightness information will be very useful in interpreting multiple binding scenarios. Table 2.3 shows the quantitative comparison between standard FCS and LFCS.

Table 2.3 comparison of resolvability of FCS and LFCS by simulation, τ_1=2ns

Sample	Major C_1 (nM)	Minor C_2 (nM)	D_2 (μm^2/ms)	S	τ_2 (ns)	χ^2
Input value	300	30	0.15	2	4	-
FCS	335±1.15e+05	10±3.57e+04	0.13±0.02	3.22±6.25e+03	NA	0.96
FCS with intensity constraint	292 ±26	35±28	0.155±0.016	1.89 ±0.37	NA	0.9
LFCS	301± 3	28± 2	0.14±0.01	2.03±0.06	4.05±0.08	1.01
FCS with lifetime and brightness linkage	300.27± 0.33	29.58±0.78	0.15± 0.01	2.01± 0.01	NA	0.98

To understand the extent to which brightness ratio S affects the two-component LFCS analysis, the relative errors of recovered fitting parameters by LFCS is studied. A series of two-component system were simulated. The concentrations C_1, C_2, diffusion coefficients D_1, D_2 of two components are kept constant as indicated in the caption, but the brightness ratio between the minor component and the major component is varied from 0.2 to 2.5.

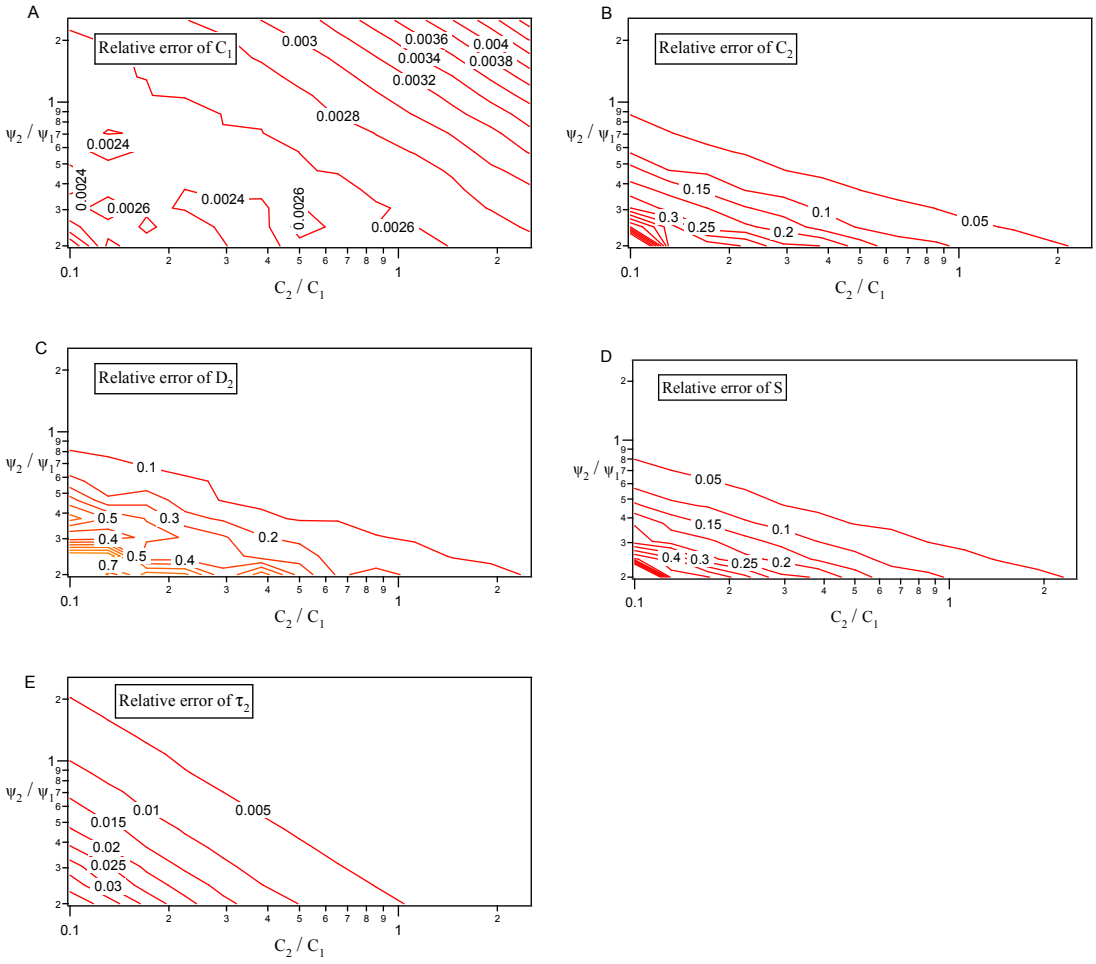

Figure 2.18: The impact of brightness ratio and concentration ratio on the resolvability of LFCS. The relative errors of C_1, C_2, D_2, S, τ_2 are plotted as a function of different brightness ratio S between the two components. Simulation parameters are C_1=300nM, D_1=0.03=D_2=0.03μm^2/ms, τ_1=4ns; τ_2=2ns, Ψ_1=5kcpsm. The relative error of (A) the major component's concentration C_1 (B) the minor component concentration C_2. (C) the diffusion coefficient D_2. (D) the brightness ratio S. (E) the lifetime of minor component τ_2.

From figure 2.18, we can learn that as the concentration of the minor component decreases, the relative error of recovering each fit parameter increases. For example, to resolve 10% minor species, the brightness ratio of the two species needs to be larger than 0.6, in order to resolve the minor species with a 10% relative error. This is caused by the fact that the brightness ratio has a

quadratic dependence in FCS function whereas the concentration is linear dependent. The minor component is more influenced by the dimmer molecular brightness than that of the major component.

As the brightness ratio increases from 1 to 2, meaning if the minor component is brighter than the major species, the relative errors of concentration, lifetime, and diffusion become less than 10%, but when the brightness ratio is less than 0.6, the errors of the recovered concentration are exceedingly large and thus make LFCS unable to resolve binary-component with satisfying accuracy. In addition, the relative errors' dependence on the concentration ratio between two components is shown.

It is worthy to point out that the relative error calculated is based on the particular diffusion coefficient and lifetime values chosen in the simulation or experiment. The more different the two lifetimes are, the less are the relative errors of each parameter and more robust resolution based on LFCS.

2.5.4.3 When the lifetime and brightness of two components are linked

In previous experiments and simulations, the molecular brightness of the major component Ψ_1 is known, thus a fixed value in LFCS analysis. When Ψ_1 is set to be a free parameter, the LFCS fit shows worse resolution (not shown). This underscores the importance of recovering Ψ_1 accurately. As we discussed in the Theory section, in a system where only one type of fluorophore is present, the molecular brightness and lifetime of two states can be linked together. And this linkage greatly increases the accuracy of LFCS even when the Ψ_1 is left to be a free parameter, as shown in the following figures.

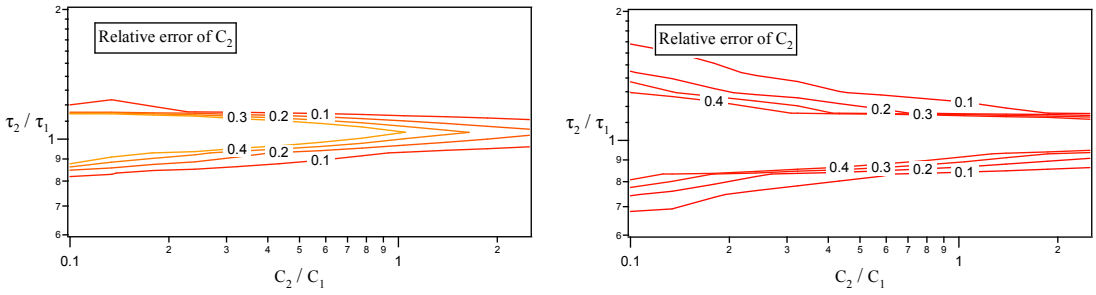

Figure 2.19: The relative error of the minor concentration C_2 when the brightness is linked with lifetime (left), when the brightness is not linked with lifetime (right). The parameter C_2 is chosen as a representative of the contrast. Other parameters are not shown for clarity.

C_1(nM)	C_2(nM)	D_1(μm^2/ms)	D_2(μm^2/ms)	Ψ_1(cpsm)	Ψ_2(cpsm)	τ_1(ns)	τ_2(ns)
300	variable	0.03	0.03	3	variable	2	variable

The improvement of accuracy from linking lifetime and brightness depends on the minor species' brightness. For smaller brightness ratios when regular LFCS shows poor resolution, the improvement by linking brightness and lifetime will more obvious. In all practical applications, the brightness ratio would be on the order of ten or less, therefore, the relative error in figure 2.13-2.19 would serve as a reference for the accuracy of LFCS analysis.

2.5.4.4 Discussion of experimental condition

Since the FCS noise is directly related to the global analysis of LFCS, a brief discussion on the FCS noise is necessary. As a critical aspect for the resolution of FCS technique, the question of statistics of FCS measurements was first studied by Koppel (Koppel, 1974). It is shown in that study that over a wide range of concentrations, the *S/N* ratio is independent of the molecular concentration, but depends strongly on the rate of photon detection per molecule, which is molecular brightness Ψ in my thesis. Based on equation (2.9), in order to optimize the signal to noise ratio in FCS, it is highly recommended to put most effort at maximizing the molecular

brightness as compared to increasing the data acquisition time, because 100 times increase in data acquisition time will only be equivalent to 10 times increase in the molecular brightness. This is extremely important when used in a photobleachable system where minimal laser illumination is desired.

The optimal condition for LFCS to resolve a minor component is to have enough signals for the minor component in the two component system. This implies that when the minor component's concentration is fewer and fewer, the molecular brightness of that component needs to be large enough to compensate for the loss of signal due to diminishing molecules, as shown quantitatively in the discussion of molecular brightness's impact, figure 2.18.

It is also worth noting that in the real experiments, the absolute concentrations in the experiments are well consistent with control experiments. As discussed by Palo (Palo et al., 2002) and Meseth (Meseth et al., 1999), because of the adhesion of the molecules to glass surfaces, they observed over 20% variation of sample's concentration in their measurements, and argued it is not adequate to determine the concentration from dilution ratios due to the imperfect/limited coating of glass chamber box. In our experiments, because of the careful coating I use, a smaller distortion of concentration is observed.

2.6 Conclusion and outlook

The objective of this work was to show that a new global analysis method, lifetime-resolved fluorescence fluctuation spectroscopy (LFCS), is achieved by combining fluorescence lifetime and fluorescence correlation function analysis together. The novel method is able to overcome the limitations of individual technique and furthermore, greatly enhance both the lifetime and diffusion based resolvability of multi-component. It was shown with simulation and experiments

that the limit of using diffusion coefficient to resolve multiple species in FCS is lifted. Even when the two components diffusion coefficients are the same, LFCS is proven to be capable of resolving two-component mixtures with an unprecedented accuracy given different lifetime values, and further discussion about the accuracy has been provided.

The combination of FCS and fluorescence lifetime analysis provides a powerful tool for studying molecular interactions in vitro and in vivo. In many practical areas, the diffusion properties of one molecule are not sensitive enough to be used to identify molecular species, the incorporation of lifetime information into species characterization expands and enhances the resolution of multi component in a heterogeneous system well beyond conventional FCS or lifetime analysis. In addition, the tolerance on deviation of LFCS is much better than FCS or lifetime only. The recovered values of fit parameters of LFCS is largely independent of the initial guess values for each fit parameters, to the contrary, FCS is heavily affected by the initial guess of fit parameters.

With the ability to overcome the molecular weight limit set by conventional FCS, LFCS now is able to be used to study small proteins' interactions with nucleic acids when they are of similar molecular weight. In our previously studied nuclear export protein Nab2 system (Kelly et al., 2007), we didn't have enough accuracy at resolving the mixture of DNA and Nab2 to determine the composition of binding complexes formed by Nab2 and short nucleic acids. It was not clear if more than one binding site of nucleic acid is available on Nab2. With the ability of accurately measuring brightness change, this LFCS technique could be applied to the Nab2 or similar systems where two interacting molecular species are of similar molecular weight. In addition, LFCS is able to provide lifetime of interacting and non-interacting species, and unlike the relative fraction yielded by FLIM, absolute concentration of each species can be obtained. As a result, it is also able to be used in FRET study now with the ability to obtain concentration information unattainable from conventional fluorescence lifetime analysis.

Chapter 3 Amyloid nanotube bundles studied by two-photon excited fluorescence and second-harmonic generation

3.1 Summary

In this chapter, we achieved the simultaneous collection of two-photon excited fluorescence (TPEF) and second-harmonic generation (SHG). The TPEF is characterized by both its emission spectrum and its fluorescence lifetime value. A new mechanism of fluorescence generation is hypothesized. A self-healing phenomenon of intrinsic fluorescence signal is found as well. The SHG signal is used to estimate the scattering length of the material. The TPEF and SHG imaging provide complementary information regarding the photophysical properties of the amyloid material.

3.2 Background

3.2.1 Formation of amyloid nanotube bundles

Short peptide models have provided novel insight into the mechanism of amyloid formation. Many short peptides have the capacity of forming typical amyloid nanotubes and fibrils *in vitro* (Gazit, 2005). It is shown that the Aβ(16-22) and Aβ(1-40) peptides form fibrils by parallel β-sheet within the fibrils found by solid state NMR and electron microscopy (Balbach et al., 2000, Paravastu et al., 2008). Aromatic interactions are important in many cases of amyloid formation (Balbach et al., 2000). In this thesis, the seven residue peptide, Aβ(16-22) (CH_3CO-KLVFFAE-NH_2), (MW 853.0), are able to form higher order structure like fibers, nanotubes, and bundles,

and we used it as a template to study the structural and photophysical properties of protein aggregations. Aβ(16-22) is an amphiphilic, cationic, core segment of the Alzheimer disease (AD) peptide, which is found to have the same ability to form plagues in human brains as standard amyloid proteins. These peptides assemble into micron long, highly homogeneous tubes under the condition of 2:3 acetonitriles:water (v:v) with 0.1% TFA at pH 2. The tubes have 52 nm cross-sectional diameters and are bounded by thin 4 nm walls (Lu et al., 2003). The peptides in the wall adopt a β-sheet conformation and are positively charged in solution due to the protonated terminal amine on the lysine side chains. The Aβ(16-22) nanotubes have been structurally determined with antiparallel one-residue shifted β sheet (Lu et al., 2003).

The self-assembling, homogeneous Aβ(16-22) can further assemble into macroscale parallel arrays through protein "salting out" strategies. In fact, the addition of Na_2SO_4, K_2SO_4, or H_2SO_4 to a solution of the Aβ(16-22) nanotubes results in the immediate formation of visible white filaments with an average diameter of ~1 μm and a contour length >5 mm (Zhou et al., 2007, Lu et al., 2007, Lu et al., 2003). Transmission electron microscopy (TEM) shows the macrofilaments to be composed of axially aligned nanotubes, and IR analysis identified tightly bound sulfate ions sequestered within the bundles.

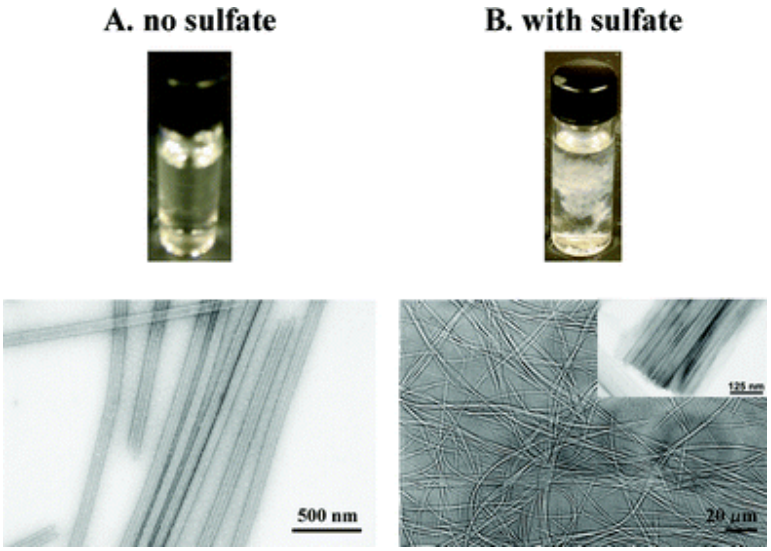

Figure 3.1: Sulfate-induced axially aligned peptide nanotube macrofilaments. (A) 2.6 mM Aβ (16–22) in 40% acetonitrile–water with 0.1% TFA (pH 2) self-assembles into highly homogeneous, soluble peptide nanotubes as measured by transmission electron microscopy (lower panel TEM). On drying, these tubes flatten to a width of 80 nm. (B) Upon addition of Na_2SO_4, the peptide nanotubes coalesce into macrofilaments, maintaining an average width of 1 μm as shown in the optical micrograph. (B lower panel inset) TEM micrograph of the macrofilaments shows the well-aligned nanotubes of the bundles, images taken from (Lu et al., 2007).

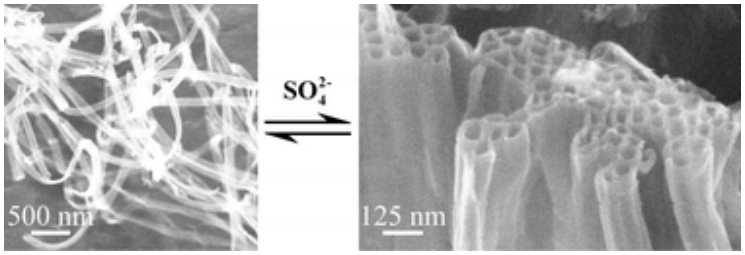

Figure 3.2: (a) The SEM images of nanotubes in the absence of sulfate. (b) The SEM images of nanotube bundles in the presence of sulfate, images taken from (Lu et al., 2007).

Although the mechanism for salt-induced protein aggregation remains poorly understood, anions induced by the sulfate are generally believed to screen electrostatic repulsion between positively charged peptide assemblies and induce short-range colligative forces (Lu et al., 2007, Lu et al., 2003).

3.2.2 Second harmonic generation (SHG)

As one of the signature techniques in multi-photon microscopy, over the last two decades, SHG has been widely used as a spectroscopic tool in a variety of interfacial studies, including liquid-

solid, liquid-air and liquid-liquid interfaces (Shen, 1984). Many of the approaches used to probe bulk interfacial properties can be extended to microscopy. This idea was first demonstrated by Hellwarth and Christensen (Hellwarth et al., 1974) and Sheppard (Sheppard et al., 1978). Because of the interfacial specificity of the process, SHG proves an excellent approach to the study of biophysics in model membranes.

Second harmonic generation (SHG) microscopy is a multi-photon detection method that carries some unique advantages over conventional fluorescence based imaging methods.
SHG is a label-free imaging method unlike any fluorescence-based methods TPEF. TPEF offers substantial advantages over other biochemical methods because of the high accuracy and non-invasive nature. However, the applications rely on the proper labeling of fluorophores onto the target biomolecules of interest since most biomolecules are not fluorescent. This poses a potential risk that the system is disturbed and artifacts are caused through the process. SHG provides ideal solution to the dilemma. In nature, SHG signals are found from a variety of extracellular structures, including collagen, microtubules, and myosin.

The properties of SHG offer several advantages for live cell or tissue imaging. Because SHG does not involve excitation of molecules, it should not suffer, in principle, from phototoxicity effects or photobleaching, both of which limit the usefulness of fluorescence microscopy, including two-photon fluorescence microscopy, for the imaging of living specimens (There can be collateral damage, however, if the incident laser light also produces two-photon excitation of chromophores in the specimen.). Excitation uses near-infrared wavelengths, allowing excellent depth penetration, and thus this method is well suited for studying thick tissue samples.

3.3 Materials and Methods

3.3.1 Lasers

The experiment setup is illustrated in Figure 2.4. Since two-photon excitations are rare events, they only occur when the laser intensity is tightly focused both in time and space, which is achieved by using an ultra fast pulsed-laser and high numerical aperture (N.A.) objective lens. In our lab, a mode-locked Tsunami Ti:sapphire laser (with pulse width of about 100 fsec and repetition rate of 80MHz, tunable between 700 to1000nm) pumped by a 532-nm 5W Millennia solid-state Nd: YVO4 laser (Spectra-Physics, Mountain View, CA) is used. An oscilloscope TDS 3032 (Tektronik, NJ) is used for monitoring laser pulses. After 4× beam expansion, the laser is sent to an Olympus inverted microscope IX71 (Olympus, Melville, NY) with an Olympus 60x water immersion objective lens (N.A.=1.2) UPLSAPO 60XW (Olympus, Melville , NY). This objective lens tightly focuses the laser to a roughly 1 fL volume and is also well corrected for chromatic aberration. We didn't choose to use an oil immersion lens, which could offer higher NA and tighter focusing, as the mismatch of the reflection index of oil and the aqueous cellular environment that could induce optical complications.

3.3.2 Laser beam scanning and imaging

For fluorescence imaging, a home-built beam scanning and imaging system was used with a software controlled motor stage ASI MS-2000 (Applied scientific instrumentation, Eugene, OR) used to move the position of interest in the sample.

3.3.3 Detectors and filters

The beam exiting the laser is deflected into the back port of the inverted IX71microscope (Olympus) and scanned across the sample by a PC-controlled galvanometer-driven x–y scanner (Series 603X, Cambridge Technology, Watertown, MA). The beam is reflected by a short-pass 675-nm dichroic beam splitter (Chroma Technology, Brattleboro, VT) and focused onto the sample. The TPEF and SHG signals from the sample are epi-collected, discriminated with the

675-nm short-pass dichroic mirror, and detected by either a photomultiplier tube (PMT) or a spectrograph.

Fluorescence signal is separated from laser light by a dichroic mirror and short pass filter before sending it to detectors. Fluorescence signal is either sent to avalanche photo diodes (APD) SPCM-AQR-13 (EG&G, Vaudreuil, Canada) for FCS measurements, or photomultiplier tubes (PMT) H7421-40 (Hamamatsu, Japan) for fluorescence imaging. Additional dichroic and filters could be placed before two APD's and/or two PMT's to separate fluorescence of different colors when performing SHG and fluorescence lifetime imaging. In all other experiments, no filters prior to the detectors are necessary.

3.3.4 TPEF and SHG acquisition

To collect the emission spectrum, the fluorescence signal was collected through a water-immersion objective directed to the back side to an optical fiber coupled spectrograph.

Spectral measurements are obtained with a SpectraPro-150 spectrograph (Roper Scientific, MA). The spectrograph has a 600 grooves per mm grating blazed at 500 nm (Acton Research, Acton, MA), and is equipped with a high dynamic range Spec-10: 400B (TE) back-illuminating CCD camera (Princeton Instruments, Trenton, NJ) which is controlled by an ST-133 Controller (Princeton Instruments). The camera has a 1340 × 400-pixel imaging array, where each pixel is a 20 × 20 μm square. The entrance slit of the spectrograph is set to a width of 0.5 mm throughout the experiments. The spectrograph and camera settings are PC-controlled through commercially available software (winspec/32 v. 2.4.6.6, Roper Scientific, Trenton, NJ). The CCD temperature is maintained to the minimum possible temperature (−40°C) for all of the experiments to ensure low dark noise. The spectra acquisition time, Δt, is 45 s.

Switching between imaging and spectra acquisition is achieved by means of changing the position of a built-in microscope mirror. When two-photon images and spectra are both obtained from the sample, the two-photon images are acquired and stored, immediately followed by emission spectra acquisition from the same depth, z, into the sample. Dark noise spectra are subtracted from the acquired sample spectra. Spectral and imaging data are imported into IgorPro for analysis and display.

3.3.5 Fluorescence lifetime imaging microscopy FLIM

Fluorescence lifetime imaging data was collected by SymPhotime software (Picoquant, Berlin, Germany). The imaging size is 256*256 pixels. Each Pixel time is 20us, frame time is 3.6s. The fluorescence lifetime measurement was calibrated by measuring the lifetime of R6G solution as well. Its standard lifetime 4.08ns was used as standard calibration before each experiment.

3.3.6 Chemicals and other materials

Rhodamine 6G (R6G) is from J.T. Baker (Phillipsburg, NJ) and rhodamine B (RB) is from ACROS organics (Geel, Belgium).

Peptide synthesis

The amyloid β(16-22) peptides were kindly provided by Yan Liang (Chemistry Department, Emory University). They were synthesized using standard FMOC peptide synthesis protocols with an Applied Biosystems ABI431 peptide synthesizer. The peptide was cleaved from the resin using the solution of TFA/thioanisole /ehtanedithiol/anisole (90/5/3/2). The peptide was then precipitated from the cleavage solution and washed repeatedly using excess ice-cold diethyl ether. Reverse phase HPLC was used for the peptide purification. The solvents used for purification

were acetonitrile and water, both of which contained 0.1% TFA. The molecular weights of the peptides were verified by MALDI mass spectroscopy.

Amyloid Nanotubes

The nanotubes were kindly provided by Yan Liang (Chemistry Department, Emory University). They were prepared under acidic condition, purified Aβ(16-22) were dissolved in 40% acetonitrile water with 0.1% TFA to a final concentration of 2mM. The peptide solution was allowed to self assemble and mature at room temperature for 2 weeks.

Amyloid nanotubes bundles

The tubes were prepared as described above. The sulfate bundles were prepared at room temperature by mixing tubes solution (2mM) and sodium sulfate solution (18mM, acetonitrile:water=2:3, v:v) with 0.1% TFA in 1/1 (v:v) ratio. After the mixing, the sulfate bundled samples were let stay overnight for fluorescence experiments.

3.4 Results and Discussion

3.4.1 Optical signals observed in amyloid nanotube bundles

To our surprise, the bundles formed by amyloid nanotubes through the 'salting out' strategy exhibit substantial optical signal upon two-photon excitation.

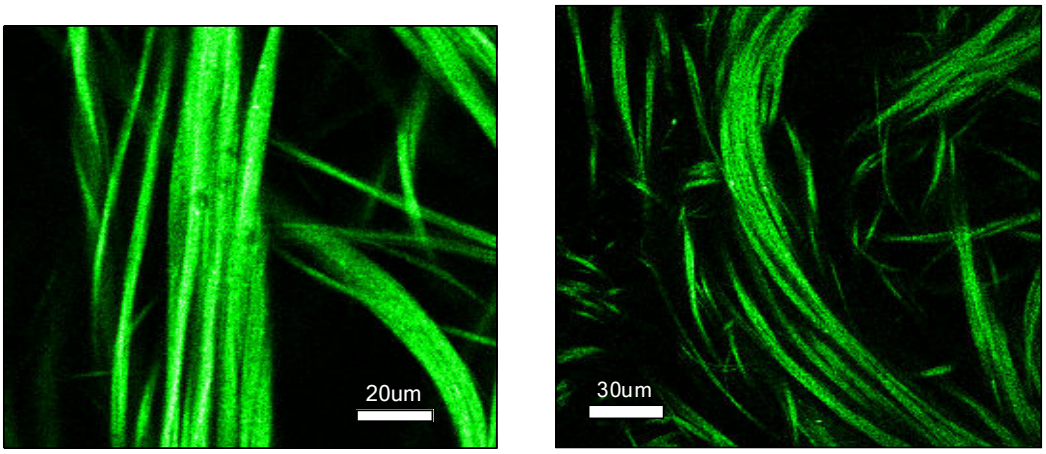

Figure 3.3: optical signals of nanotube bundles under two-photon excitation. λ=780nm. Pixel time is 20 μs.

Consistent with SEM results, the bundles adopt a ribbon shape structure with diameters ranging from 2-40μm, the axial length is over 100 μm. Kinks and swirls pattern is visible. This type of signal is detectable in a range of 200μm in the z direction.

This strong optical signal intrigued us greatly because there was no fluorescent dye introduced to the peptides. When the nanotubes are formed in the solution without bundling, these nanotubes didn't exhibit optical signals under the same excitation. Only when sulfate was added into the nanotube solution, these bundles were formed into these ribbon shape structure and optical signals were observed.

To understand what the signal is and how the amyloid nanotubes interact with light, we aimed to use two-photon excitation spectroscopy and microscopy to investigate its photophysical properties.

3.4.2 Characterization of image-forming signal

The first step is to characterize its emission properties. At excitation wavelength λ=780nm, the emission spectrum is measured by our spectrograph and shown in figure 3.4.

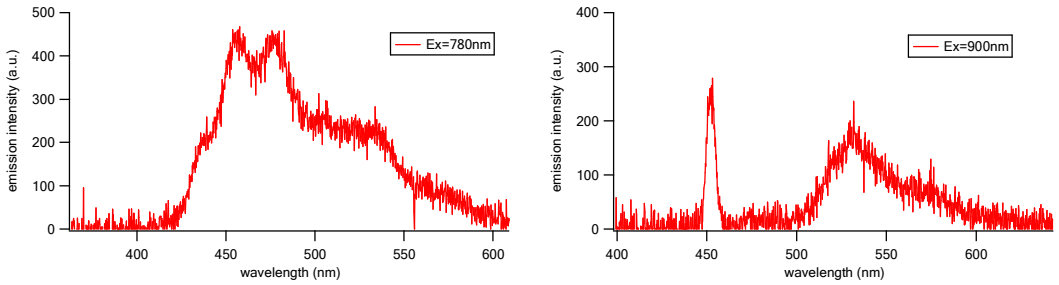

Figure 3.4: the emission spectrum of amyloid nanobutes bundles in solution under two photon excitation λ=780nm (left), λ=900nm (right).

It is apparent that under 780nm excitation this optical signal is two-photon excited fluorescence (TPEF), in the visible green-blue range of visible light. Two primary peaks are visible: one is around 470nm and another at 540nm. Interestingly, under 900nm excitation, there is a strong peak at around 450nm. This signal is comparable with the TPEF intensity. Given its position at half the excitation wavelength, we hypothesize that it is second harmonic generation signal, which is probed further in following sections. A more systematic laser tuning shows that the emission spectrum of intrinsic fluorescence shows variations depending on different excitation wavelength.

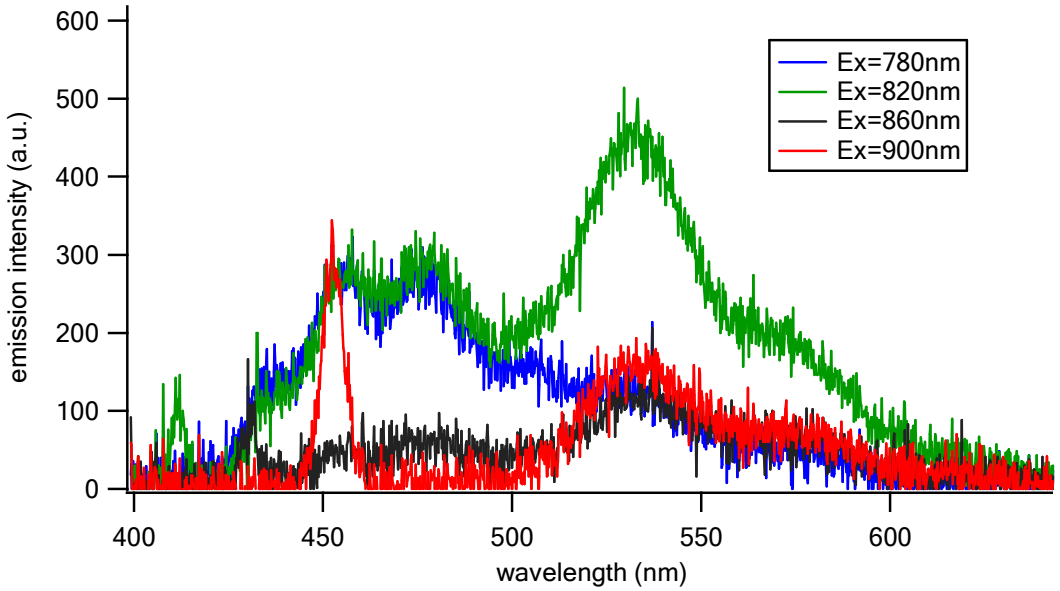

Figure 3.5: the emission Spectrum of the nanotubes bundles at different excitation wavelength λex=780nm, 820nm, 860nm, 900nm.

Due to the fact that no external fluoresce label is used in imaging, the origin of this intrinsic fluorescence is of particular interests to the medical field because the label-free strategy in imaging has long been wanted to diagnose diseases and its relations with structural and functional changes.

3.4.3 Fluorescence lifetime study

Fluorescence lifetime is a widely used technique to characterize photophysical properties of biological samples. Here fluorescence lifetime measurements were done to characterize the bundles photophysical properties.

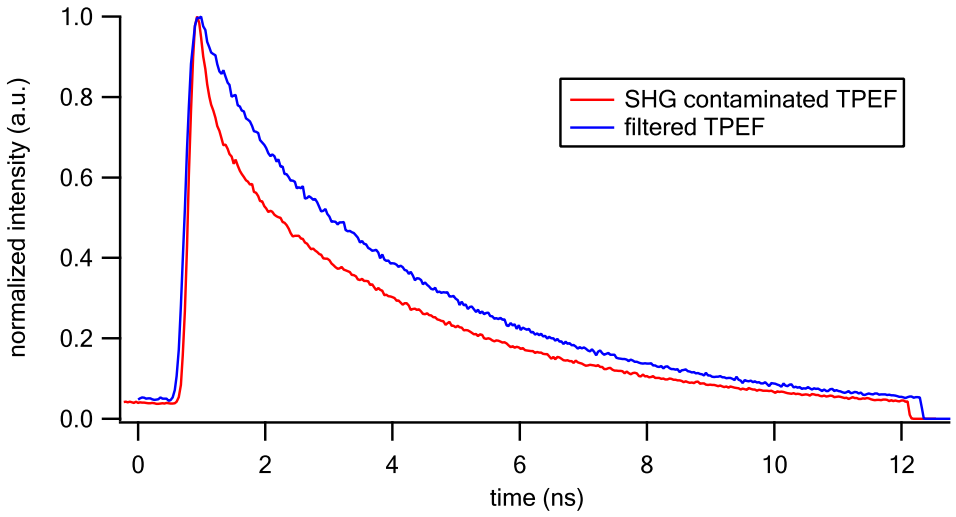

Figure 3.6: the lifetime fit of SHG contaminated decay and filtered fluorescence decay.

Because of the SHG signal in the collected optical signal, we need to use optical filters to remove the SHG signals. SHG is an instantaneous process upon excitation of laser pulses, therefore, it show as instantaneous decay at the onset of fluorescence lifetime decay. This contamination has to be excluded from both data acquisition and data analysis for minimal data distortion.

Considering the two apparent emission peaks at 450-500nm and 500-700nm, the fluorescence emission are collected sequentially by two sets of filters, 480/30 and 530/50 as only one detector is available. In order to thoroughly understand the photophysical properties, a series of excitation wavelengths are chosen to excite the amyloid sample and the corresponding fluorescence lifetimes are measured.

Table 3.1 the lifetime of bundles from 465-495nm emission

Samples	Excitation (nm)	Single-component lifetime (ns)
Aβ(16-22)	780	3.8±0.10
Aβ(16-22)	820	3.73±0.11

Aβ(16-22)	860	3.62±0.05
Aβ(16-22)	895	NA

Table 3.2 the lifetime of bundles from 505-700nm emission, to include the 2nd peak

Samples	Excitation (nm)	Single-component lifetime (ns)
Aβ(16-22)	780	3.65±0.03
Aβ(16-22)	820	3.66±0.04
Aβ(16-22)	860	3.46±0.06
Aβ(16-22)	895	3.5±0.04

Table 3.3 the lifetime of Rhodamine 6G

Sample	Excitation (nm)	Single-component lifetime (ns)
Rhodamine 6G	780nm	3.95±0.06
Rhodamine 6G	820nm	3.93±0.03
Rhodamine 6G	860nm	3.9±0.04
Rhodamine 6G	895nm	3.88±0.04

Rhodamine 6G serves as the controls for lifetime comparison at different excitation wavelengths. It is seen that within the experimental errors, the two emission peaks of nanotube bundles are not distinctive based on fluorescence lifetime values.

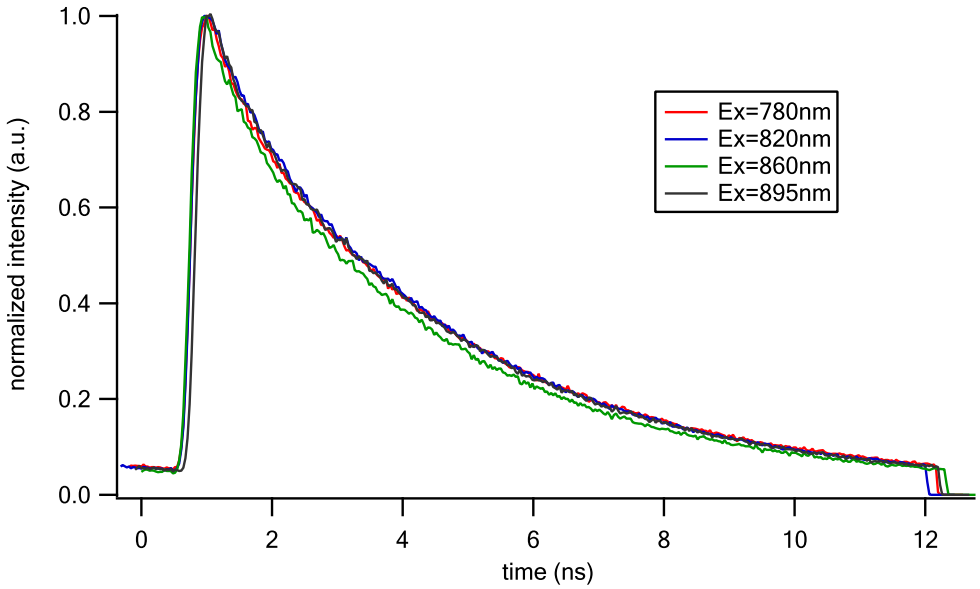

Figure 3.7: lifetime decay at different excitation wavlengths, 780nm, 820nm, 860nm and 900nm of the Aβ(16-22) nanotube bundles. The intensity is normalized.

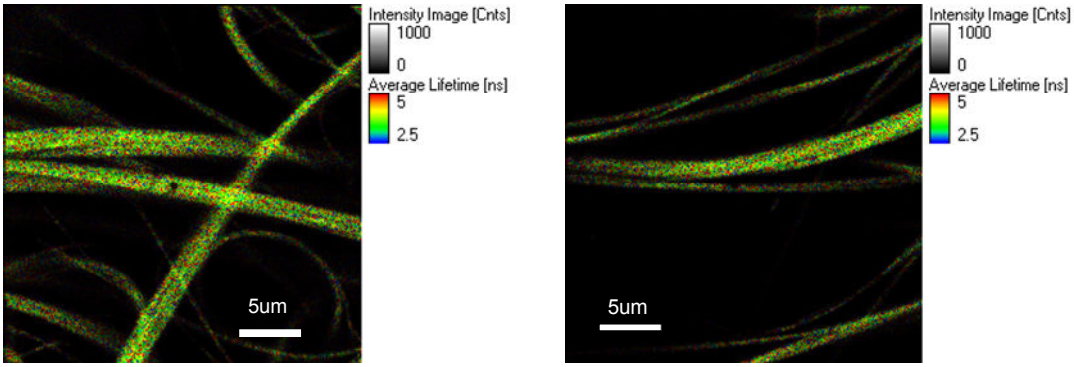

Figure 3.8: fluorescence lifetime imaging of nanotube bundles, 780nm excitation (left) and 820nm excitation (right).

The measured lifetime imaging doesn't indicate complex fluorescence pattern at different location of the sample, and the uniformed value implies a uniform relaxation of excited energy. It suggests that the origin of the intrinsic fluorescence is from highly homogenous and ordered structure of the nanotube bundles, which is consistent with the homogenous cross-β sheet

structure in the nanotube formation. This ordered structure is also shown to be able to generate SHG signal as will be discussed later in the chapter.

3.4.4 Strong evidence for solvent-assisted fluorescence

During our initial test, it was observed that the fluorescence signals usually decrease to an immeasurable level within days after the bundles samples were mounted on the cover slip, suggesting that the sample was degrading in term of its structure and subsequently caused its photophysical spectral change.

The finding of possible involvement of moisture level in the sample's fluorescence property, we construct a sealed coverglass with a hole 1mm in diameter drilled in the middle, so we were able to control the environment of the amyloid by adding water or drying the sample.

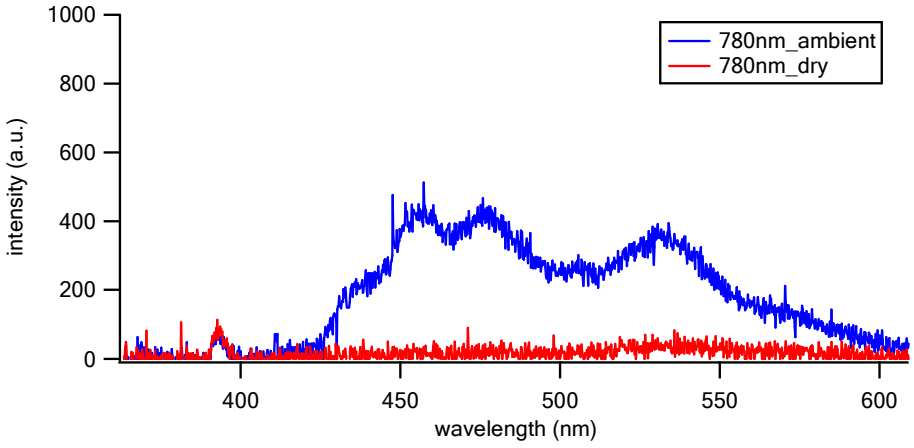

Figure 3.9: the emission spectrum of bundles at excitation wavelength 780nm. Power 4.64mW at 780nm excitation.

In the figure 3.9, green-blue emission is apparent at 780nm excitation wavelength when the sample is newly prepared which is immersed in the solvent as described in the method section. The emission is predominately intrinsic fluorescence 470-560nm. When the sample is dried, the fluorescence signal drops to near zero, this strongly suggest a possible role of water molecules in the generation of fluorescence.

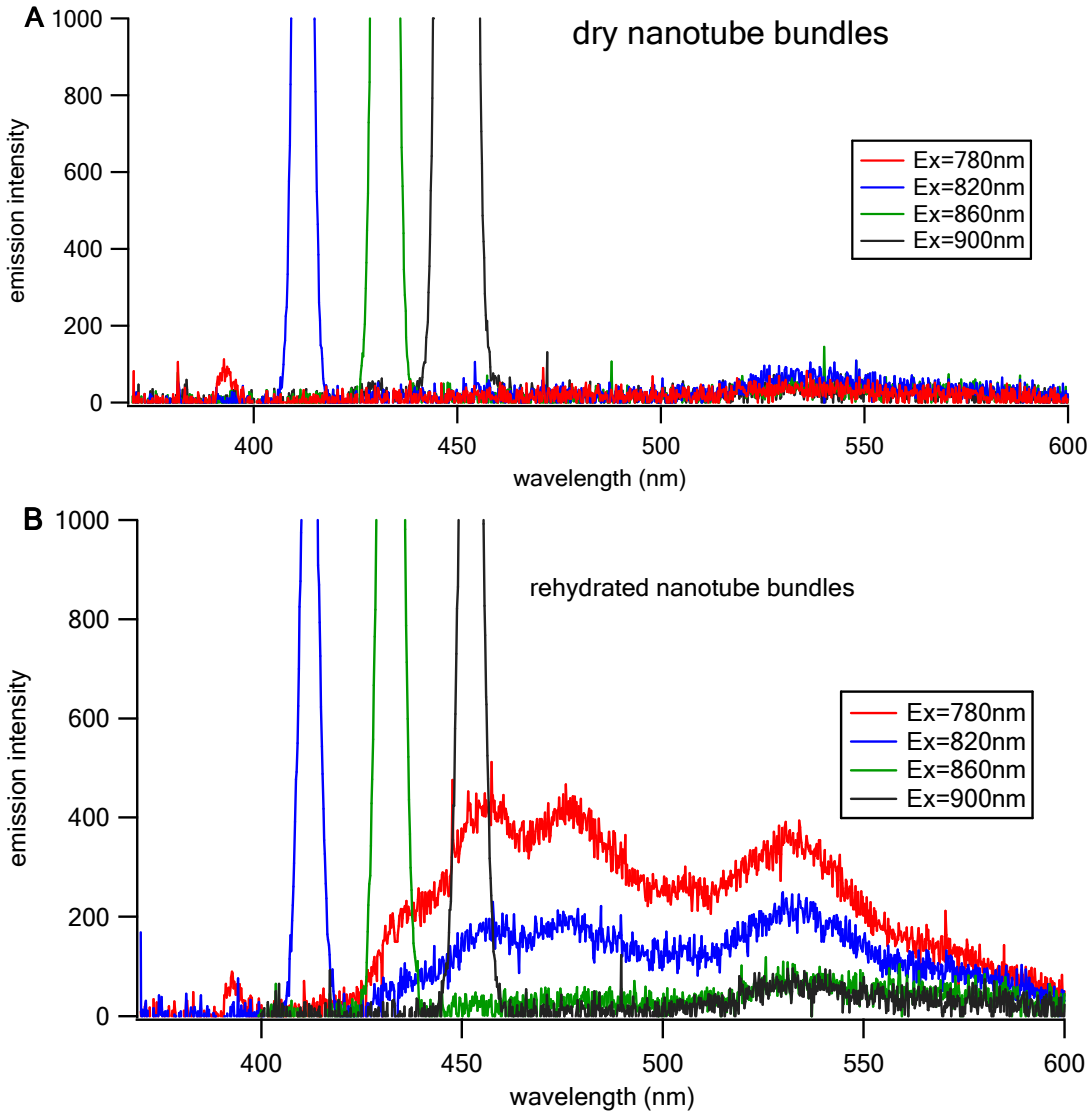

Figure 3.10: the emission spectra obtained from both dry and rehydrated nanotube bundles fro λex= 780nm, 820nm, 860nm, 900nm for acquisition time =45s. The excitation power before and after rehydration is kept the same.

As a validation of water's involvement, water was added back to the sample, and the subsequent spectroscopic measurement in figure 3.10 confirmed that substantial fluorescence was recovered. This observation provides the evidence that water molecules play a significant role in the origin of intrinsic fluorescence.

Our observation of intrinsic fluorescence and its dependence on the moisture level is in good agreement with another newly found intrinsic fluorescence from amyloid like fibrils formed by polypeptide (del Mercato et al., 2007). In their experiment, each fibril consists of several protofilaments arranged in a roughly twisted pattern, indicating that they were formed through the lateral alignment of many polypeptide molecules. The diameter of the fibrils was in the range of 20-250nm and when they laterally aggregate, the diameter increase to around 1um. They observed green-blue fluorescence signal which has a broad peak around 460nm. This fluorescence signal is also strongly related to the ambient condition of water molecules (del Mercato et al., 2007). The authors argued that this change in fluorescence intensity coupled with the material's varied conductivity properties suggests a delocalization mechanism in which electrons are delocalized by extensive hydrogen bonding in the cross-β network in the fibrils. It is also reported by Zipfel that beta-amyloid plaque don't exhibit autofluorescence, but the neurofibrillary tangle location of β-amyloid in Alzheimer Disease display fluorescence emission centered at 460nm under 2PE at 700-800nm excitation (Zipfel et al., 2003). The resulted emission peak (460nm) is redder than expected peak from ditryosine alone (400nm). It is hypothesized that it is caused by higher order polymerized tyrosine products (Mahmoud et al., 1995). Similar fluorescence behavior in the normally non-fluorescent peptide system is also found recently by

another group (Guptasarma, 2008). They proposed a theory in which the hydrogen bonding in the proteins is responsible for the delocalization of electrons which lowers the energy for excitation for visible emission.

It is possible that in our amyloid nanotube structure, the intrinsic fluorescence is caused by the same mechanism. The electrons are delocalized when peptide bonds engage in hydrogen bonding, which enables the electrons available for visible regions of the spectrum by means of networks of peptides and hydrogen bonds. The increase of conjugation assisted by water molecules leads to red-shift in emission. When water molecules are lost from the bundled structures, hydrogen bonds between tubes collapse and, in turn, electronic delocalization is strongly reduced. This hypothesis could be confirmed by electronic charge study to compare conductivity at both dry and wet condition of amyloid bundles.

3.4.5 Applications of SHG

SHG has been applied to studied many interesting biological systems. For example, the process of tumor cell migration along collagen fibers can be observed by using GFP-labeled tumor cells and intrinsic collagen SHG (Zipfel et al., 2003). 2PE fluorescence spectra currently exist for NAD(P)H and some flavins (Huang et al., 2002, Xu et al., 1996), and 3PE spectra exist for serotonin, tryptophan, and dopamine (Zipfel et al., 2003).

In this section, I present the combined use of TPEF and SHG in reflection mode to obtain complementary information that allows noninvasive, spatially localized in-vitro characterization of amyloid tube aggregates. We also present studies utilizing SHG signal from the sample to probe its structural information.

3.4.6 Spectroscopic study of SHG

Figure 3.5 shows the emission spectrum of bundles. Besides some broad peaks at 470nm and 530nm, there is an apparent narrow peak at 450nm under 900nm two-photon excitation. To determine whether the origin of the strong peak signal is SHG or not, the Ti-Sapphire laser was tuned to various excitation wavelengths, λ_{ex}, throughout its tuning range. The emission spectra were acquired and shown in figure 3.11.

When the bundle samples are dry, the emission spectra reveal strong second harmonic generation SHG signals for the excitation wavelengths >820nm, manifested by a narrow peak at half the excitation wavelength.

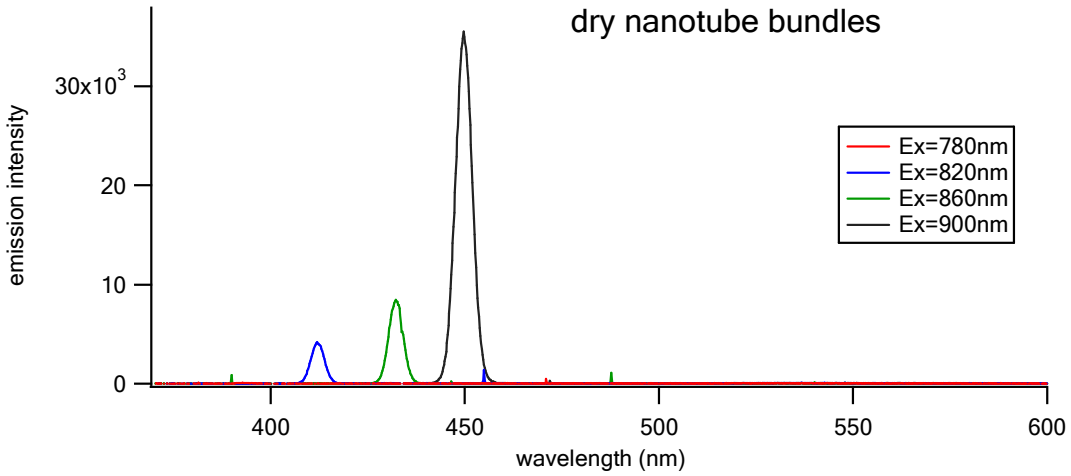

Figure 3.11: emission spectra showing the SHG signal at different excitation wavelengths.

It is clearly shown that the sharp peak in emission is SHG signal as it precisely follows the half of the excitation wavelength. The ability to shift λ_{SHG} by tuning the excitation wavelength λ_1 has practical implications for tissue imaging because SHG can always be distinctively separated from other emissions.

3.4.7 Imaging contrast between TPEF and SHG

This endogenous imaging is of great significance because SHG originates within the proteins of interest encoding information on molecular orientation and assembly that cannot be elicited from the fluorescence of exogenous labeling such as GFP.

GFP has been very successful in noninvasive study of biological systems, but it usually is attached to the molecule of interest with a certain length of linker, thus displays flexibility when used in polarization study. Information regarding the anisotropy and radial and lateral distribution is lost from GFP imaging.

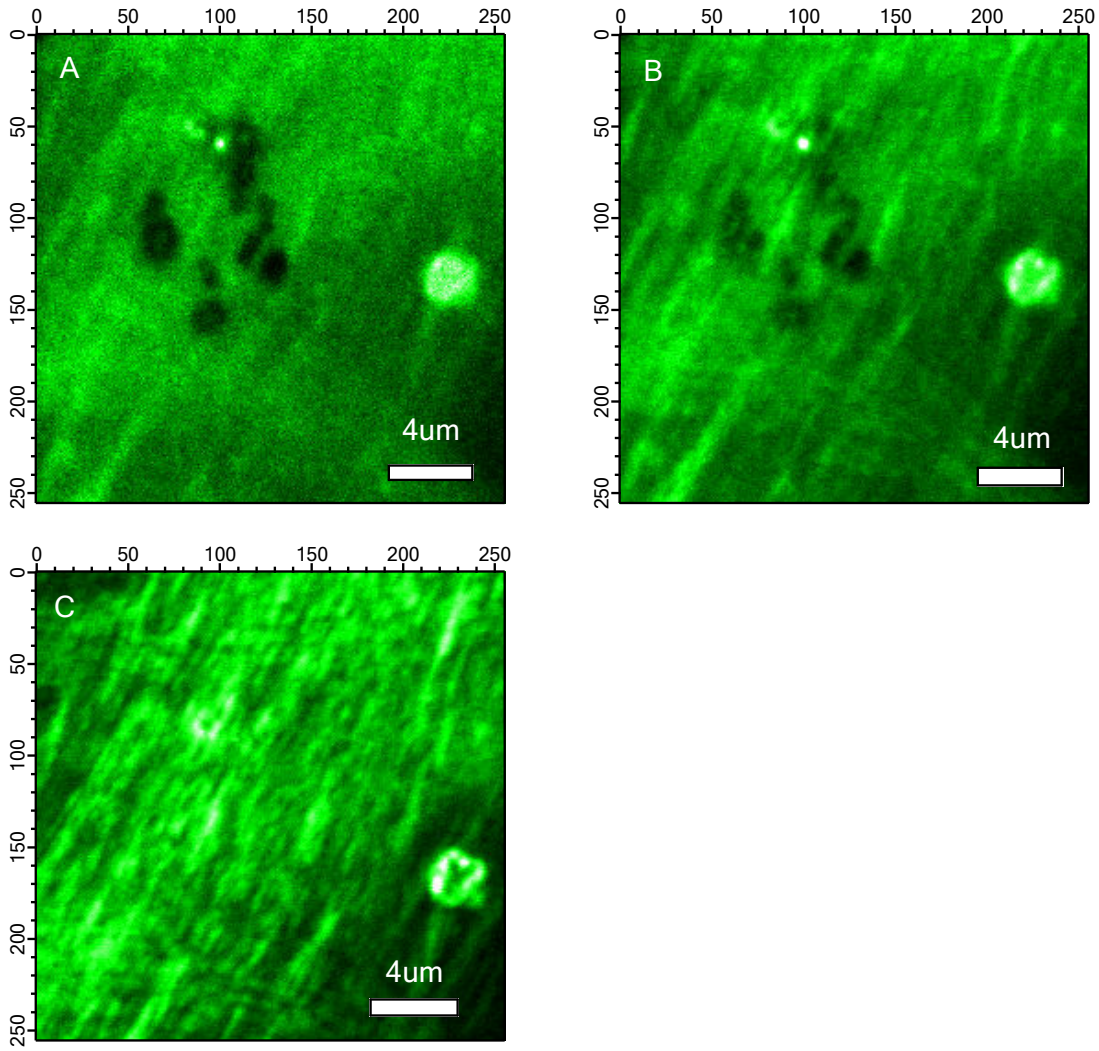

Figure 3.12: the images of nanotube bundles under two-photon excitation at A: 780nm B: 820nm, C: 900nm excitation. As discussed in previous section, A is mainly composed of intrinsic fluorescence signal. B is a combination of TPEF and SHG. C is mainly SHG signal.

In the figure 3.12A, where Ex=780nm, the emission is mostly fluorescence signal, the dark spots due to photobleaching are visible, however, as the excitation wavelength is tuned to longer wavelengths, 820nm and 900nm, the photobleaching effect is compensated by the strong SHG signal. At λ=900 nm, the fine structure of amyloid tube bundles are seen. This observation sheds light to a very interesting question: even though the photophysical properties of amyloid are destructed by the two photon absorption, the hollow tube is still capable of generating SHG signal through non-absorptive process suggesting the fundamental noncentro-symmetric structure is still preserved.

Another interesting observation of the optical signal is that at 780-800nm, the sample exhibit dominant fluorescence signal as shown in figure 3.5, and two-photon imaging shows blurring effect from the whole image. In contrast, at longer excitation 860-900nm, the dominant signal is back-scattering SHG, and although the SHG signal intensity is comparable with the fluorescence imaging, the signal is no longer blurring, to the contrary, it reveal rather crisp pattern within the tubes bundles.

3.5 Significance of the finding

Optical properties of biological molecules contain important information about their structure and function (Merino et al., 2008, Wouters et al., 2001). This technique and finding is significant for studying molecular self-assembly. How the amyloid peptides is able to assembly into higher order structure and generate blue-green fluorescence signal will be significant in both biological and

medical research and also in nano-sized optical device and biosensors (Gazit, 2007, Reches et al., 2006). In each amyloid disease, the fibrils are formed by a different polypeptide, develop in the affected tissue, and contribute to cell death by mechanisms that are not entirely known (Paravastu et al., 2008, Petkova et al., 2005). Other studies have suggested that any proteins can form fibrils (Wetzel et al., 2006). This fact that amyloid formation does not strongly depend on amino acid sequence illuminates the significance and potential scope of this study. Biological samples usually are not conductive, so our observation of fluorescence from nanotube bundles formed by peptides is a significant finding that shows potentials for future biological based electronics. Understanding the fluorescence phenomenon of these materials would lead to deeper understanding in the conduction properties of these protein materials, namely, biological conductor, with great potentials in the nano-sized high performance computing, artificial materials, optical device, electronical device, etc. These ordered nanostructures are ideal for fabricating novel bio-inspired materials. Future comparison of conductivity could be made in relevant to carbon nanotubes, which shows superior conductivity and have been found highly attracting for fabricating solar cells (Li et al., 2007) and next-generation bio-batteries (Lee et al., 2009).

3.6 Summary and future effort

Although not specifically investigated in this work, the unique sensitivity of MPM suggests the potential of the technique to monitor noninvasively the state of amyloid aggregates. Possible applications of this technology could include detecting and tracking the progression of amyloid pathologies in human brain as well as monitoring the effect of surgical procedures.

The combined use of TPEF and SHG imaging not only provides a useful means of assessing morphological and photophysical features of nanotube scaffolds, but it also allows distinction of

the amyloid bundle features from those of other extracellular matrix proteins that generate autofluorescence because we can easily tune the excitation wavelength to separate the SHG signal from other autofluorescence sources. This may prove useful in future in-vivo diagnosis of amyloid aggregation in human brains.

In the future, a forward condenser may also be needed to measure the ratio of forward SHG over backward SHG to understand more structural details. It could be used to access the hydration conditions like in the case of collagen (Williams et al., 2005).

Chapter 4 Outlook

In this thesis, two topics are covered. The first is the novel analysis method, namely lifetime-resolved fluorescence correlation spectroscopy (LFCS). The second is the spectroscopic and microscopic study of amyloid nanobute bundles.

In recent years much progress has been made to increase the amount of information that can be retrieved from the collected fluorescence trace. Upon extension of the FCS equipment additional parameters such as molecular brightness, spectral characteristics and anisotropy could be retrieved (Chen et al., 1999, Palo et al., 2002, Eggeling et al., 2001). The ultimate goal of the study presented in chapter 2 is to extend current FCS methodology and develop a technique that is able to monitor the molecular interactions with better accuracy or furthermore, extends to *in vivo* studies. To describe the complicated dynamical processes and molecular interactions occurring within the living cells more advanced fit models are required to analyze the experimental data (Gennerich et al., 2000). Thanks to the sensitive, selective and non-invasive properties of fluorescence based methodologies, this LFCS combines the advantages of FCS and fluorescence lifetime, thus holds great potential to be applied in the near future to *in vivo* study. There are, however, limitations and caveats associated with this technique in applying to the

living cells. Intracellular experiments may be complicated by the presence of autofluorescence (Aubin, 1979, Andersson et al., 1998). Scattering of the light, due to the presence of optically dense structures in cells, will also drastically reduce the signal to noise ratio. In addition, the anomalous diffusive properties of molecules inside cells may introduce new fitting parameters thus new obstacles. Nonetheless, the thesis presented the fundamental step towards future applications in more complex systems.

In a separate project which is presented in chapter 3, we discovered the intrinsic fluorescence phenomenon in the amyloid materials. A self-healing phenomenon of intrinsic fluorescence signal and SHG signal is found. The mechanism of fluorescence generation is discussed. Conductivity and mechanical measurements should be carried out in the future to measure the electron conductivity and mechanical properties of this amyloid material. The correlation between the amyloid's photo-electronic properties and its structure will also be interesting and significant not only to a big audience in medical field, but also in material and engineering field. Deeper understanding of the photophysical properties of amyloid materials will undoubtedly contribute to the developments of bio-inspired materials and possibly shed light to the diagnosis of relevant diseases and next generation materials science.

List of References:

Andersson, H., Baechi, T., Hoechl, M. and Richter, C. 1998. Autofluorescence of living cells. *Journal of Microscopy* 191**:**1-7.

Aubin, J. E. 1979. Autofluorescence of viable cultured mammalian cells. *Journal of Histochemistry and Cytochemistry* 27**:**36-43.

Balbach, J. J., Ishii, Y., Antzutkin, O. N., Leapman, R. D., Rizzo, N. W., Dyda, F., Reed, J. and Tycko, R. 2000. Amyloid Fibril Formation by Aβ16-22, a Seven-Residue Fragment of the Alzheimer's β-Amyloid Peptide, and Structural Characterization by Solid State NMR. *Biochemistry* 39**:**13748-13759.

Barber, P. R., Ameer-Beg, S. M., Gilbey, J. D., Edens, R. J., Ezike, I. and Vojnovic, B. 2005. Global and pixel kinetic data analysis for FRET detection by multi-photon time-domain FLIM. IN P. Ammasi and T. C. S. Peter (Eds.). SPIE.

Bastiaens, P. I. H. and Squire, A. 1999. Fluorescence lifetime imaging microscopy: spatial resolution of biochemical processes in the cell. *Trends in Cell Biology* 9**:**48-52.

Berland, K. M., So, P. T., Chen, Y., Mantulin, W. W. and Gratton, E. 1996. Scanning two-photon fluctuation correlation spectroscopy: particle counting measurements for detection of molecular aggregation. *Biophysical Journal* 71**:**410-420.

Berland, K. M., So, P. T. and Gratton, E. 1995. Two-photon fluorescence correlation spectroscopy: method and application to the intracellular environment. *Biophysical Journal* 68**:**694-701.

Butt, H.-J., Cappella, B. and Kappl, M. 2005. Force measurements with the atomic force microscope: Technique, interpretation and applications. *Surface Science Reports* 59**:**1-152.

Chen, Y., Muller, J. D., Ruan, Q. and Gratton, E. 2002. Molecular Brightness Characterization of EGFP In Vivo by Fluorescence Fluctuation Spectroscopy. *Biophys. J.* 82**:**133-144.

Chen, Y., Muller, J. D., So, P. T. C. and Gratton, E. 1999. The photon counting histogram in fluorescence fluctuation spectroscopy. *Biophysical Journal* 77**:**553-567.

Chen, Y., Wei, L. N. and Muller, J. D. 2003. Probing protein oligomerization in living cells with fluorescence fluctuation spectroscopy. *Proceedings of the National Academy of Sciences of the United States of America* 100**:**15492-15497.

Del Mercato, L. L., Pompa, P. P., Maruccio, G., Della Torre, A., Sabella, S., Tamburro, A. M., Cingolani, R. and Rinaldi, R. 2007. Charge transport and intrinsic fluorescence in amyloid-like fibrils. *Proceedings of the National Academy of Sciences of the United States of America* 104**:**18019-18024.

Eggeling, C., Berger, S., Brand, L., Fries, J. R., Schaffer, J., Volkmer, A. and Seidel, C. A. M. 2001. Data registration and selective single-molecule analysis using multi-parameter fluorescence detection. *Journal of Biotechnology* 86**:**163-180.

Eigen, M. and Rigler, R. 1994. Sorting single molecules: application to diagnostics and evolutionary biotechnology. *Proceedings of the National Academy of Sciences of the United States of America* 91**:**5740-5747.

Elson, E. L. 2001. Fluorescence correlation spectroscopy measures molecular transport in cells. *Traffic* 2**:**789-796.

Elson, E. L. and Magde, D. 1974. Fluorescence correlation spectroscopy. I. Conceptual basis and theory. *Biopolymers* 13**:**1-27.

Enderlein, J. and Gregor, I. 2005. Using fluorescence lifetime for discriminating detector afterpulsing in fluorescence-correlation spectroscopy. *Review of Scientific Instruments* 76**:**033102.

Frommer, J. 1992. Scanning Tunneling Microscopy and Atomic Force Microscopy in Organic Chemistry. *Angewandte Chemie International Edition in English* 31**:**1298-1328.

García, R. and Pérez, R. 2002. Dynamic atomic force microscopy methods. *Surface Science Reports* 47**:**197-301.

Gazit, E. 2005. Mechanisms of amyloid fibril self-assembly and inhibition. *FEBS Journal* 272**:**5971-5978.

Gazit, E. 2007. Self Assembly of Short Aromatic Peptides into Amyloid Fibrils and Related Nanostructures. *Prion* 1**:**32-35.

Gennerich, A. and Schild, D. 2000. Fluorescence correlation spectroscopy in small cytosolic compartments depends critically on the diffusion model used. *Biophysical Journal* 79**:**3294-3306.

Gough, A. H. and Taylor, D. L. 1993. Fluorescence anisotropy imaging microscopy maps calmodulin binding during cellular contraction and locomotion. *J. Cell Biol.* 121**:**1095-1107.

Grecco, H. E., Roda-Navarro, P. and Verveer, P. J. 2009. Global analysis of time correlated single photon counting FRET-FLIM data. *Optics Express* 17**:**6493-6508.

Gregor, I. and Enderlein, J. 2007. Time-resolved methods in biophysics. 3. Fluorescence lifetime correlation spectroscopy. *Photochemical & Photobiological Sciences* 6**:**13 - 18.

Guptasarma, P. 2008. Solution-state characteristics of the ultraviolet A-induced visible fluorescence from proteins. *Archives of Biochemistry and Biophysics* 478**:**127-129.

Hansma, P. K. and Tersoff, J. 1987. Scanning tunneling microscopy. *Journal of Applied Physics* 61**:**R1-R24.

Hellwarth, R. and Christensen, P. 1974. Nonlinear optical microscopic examination of structure in polycrystalline ZnSe. *Optics Communications* 12**:**318-322.

Hess, S. T., Huang, S., Heikal, A. A. and Webb, W. W. 2001. Biological and Chemical Applications of Fluorescence Correlation Spectroscopy: A Review. *Biochemistry* 41**:**697-705.

Huang, S. H., Heikal, A. A. and Webb, W. W. 2002. Two-photon fluorescence spectroscopy and microscopy of NAD(P)H and flavoprotein. *Biophysical Journal* 82**:**2811-2825.

Kelly, S. M., Pabit, S. A., Kitchen, C. M., Guo, P., Marfatia, K. A., Murphy, T. J., Corbett, A. H. and Berland, K. M. 2007. Recognition of polyadenosine RNA by zinc finger proteins. *Proceedings of the National Academy of Sciences of the United States of America* 104**:**12306-12311.

Koppel, D. E. 1974. Statistical accuracy in fluorescence correlation spectroscopy. *Physical Review A* 10**:**1938.

Koppel, D. E., Axelrod, D., Schlessinger, J., Elson, E. L. and Webb, W. W. 1976. Dynamics of fluorescence marker concentration as a probe of mobility. *Biophysical Journal* 16**:**1315-1329.

Kral, T., Langner, M., Benes, M., Baczynska, D., Ugorski, M. and Hof, M. 2002. The application of fluorescence correlation spectroscopy in detecting DNA condensation. *Biophysical Chemistry* 95**:**135-144.

Krichevsky, O. and Bonnet, G. 2002. Fluorescence correlation spectroscopy: the technique and its applications. *Reports on Progress in Physics* 65**:**251-297.

Lakowicz, J. R. 2006a. *Principles of Fluorescence Spectroscopy* New York: Springer.

Lakowicz, J. R. 2006b. *Principles of Fluorescence Spectroscopy, 3rd Ed.* New York: Springer.

Lee, Y. J., Yi, H., Kim, W.-J., Kang, K., Yun, D. S., Strano, M. S., Ceder, G. and Belcher, A. M. 2009. Fabricating Genetically Engineered High-Power Lithium-Ion Batteries Using Multiple Virus Genes. *Science* 324**:**1051-1055.

Li, C., Chen, Y. H., Wang, Y. B., Iqbal, Z., Chhowalla, M. and Mitra, S. 2007. A fullerene-single wall carbon nanotube complex for polymer bulk heterojunction photovoltaic cells. *Journal of Materials Chemistry* 17**:**2406-2411.

Lu, K., Guo, L., Mehta, A. K., Childers, W. S., Dublin, S. N., Skanthakumar, S., Conticello, V. P., Thiyagarajan, P., Apkarian, R. P. and Lynn, D. G. 2007. Macroscale assembly of peptide nanotubes. *Chemical Communications***:**2729-2731.

Lu, K., Jacob, J., Thiyagarajan, P., Conticello, V. P. and Lynn, D. G. 2003. Exploiting amyloid fibril lamination for nanotube self-assembly. *Journal of the American Chemical Society* 125**:**6391-6393.

Ma, G. B., Mincu, N., Lesage, F., Gallant, P. and Mcintosh, L. 2005. System IRF impact on fluorescence lifetime fitting in turbid medium. *Imaging, Manipulation, and Analysis of Biomolecules and Cells: Fundamentals and Applications III* 5699**:**263-273.

Magde, D. 1976. Chemical Kinetics and Fluorescence Correlation Spectroscopy. *Quarterly Reviews of Biophysics* 9**:**35-47.

Magde, D., Elson, E. L. and Webb, W. W. 1974. Fluorescence correlation spectroscopy. II. An experimental realization. *Biopolymers* 13**:**29-61.

Mahmoud, S. F. and Bialkowski, S. E. 1995. Laser-excited fluorescence of dityrosine. *Applied Spectroscopy* 49**:**1669-1676.

Merino, E. J., Boal, A. K. and Barton, J. K. 2008. Biological contexts for DNA charge transport chemistry. *Current Opinion in Chemical Biology* 12**:**229-237.

Meseth, U., Wohland, T., Rigler, R. and Vogel, H. 1999. Resolution of Fluorescence Correlation Measurements. *Biophysical Journal* 76**:**1619-1631.

Muller, J. D., Chen, Y. and Gratton, E. 2000. Resolving heterogeneity on the single molecular level with the photon-counting histogram. *Biophysical Journal* 78**:**474-486.

Palo, K., Brand, L., Eggeling, C., Jäger, S., Kask, P. and Gall, K. 2002. Fluorescence Intensity and Lifetime Distribution Analysis: Toward Higher Accuracy in Fluorescence Fluctuation Spectroscopy. *Biophysical Journal* 83**:**605-618.

Paravastu, A. K., Leapman, R. D., Yau, W. M. and Tycko, R. 2008. Molecular structural basis for polymorphism in Alzheimer's beta-amyloid fibrils. *Proceedings of the National Academy of Sciences of the United States of America* 105**:**18349-18354.

Petkova, A. T., Leapman, R. D., Guo, Z., Yau, W.-M., Mattson, M. P. and Tycko, R. 2005. Self-Propagating, Molecular-Level Polymorphism in Alzheimer's {beta}-Amyloid Fibrils. *Science* 307**:**262-265.

Reches, M. and Gazit, E. 2006. Molecular self-assembly of peptide nanostructures: mechanism of association and potential uses. *Current Nanoscience* 2**:**105-111.

Rigler, R. and Elson, E. 2000. *Fluorescence Correlation Spectroscopy: Theory and Applications.* New York: Springer.

Schwille, P. and Heinze, K. G. 2001. Two-Photon Fluorescence Cross-Correlation Spectroscopy. *ChemPhysChem* 2**:**269-272.

Schwille, P., Meyer-Almes, F. J. and Rigler, R. 1997. Dual-color fluorescence cross-correlation spectroscopy for multicomponent diffusional analysis in solution. *Biophysical Journal* 72**:**1878-1886.

Sengupta, P., Garai, K., Balaji, J., Periasamy, N. and Maiti, S. 2003. Measuring size distribution in highly heterogeneous systems with fluorescence correlation spectroscopy. *Biophysical Journal* 84**:**1977-1984.

Shen, Y. R. 1984. *The principles of nonlinear optics.* New York: Wiley.

Sheppard, C. J. R. and Kompfner, R. 1978. Resonant scanning optical microscope. *Applied Optics* 17**:**2879-2882.

Skakun, V. V., Hink, M. A., Digris, A. V., Engel, R., Novikov, E. G., Apanasovich, V. V. and Visser, A. J. W. G. 2005. Global analysis of fluorescence fluctuation data. *European Biophysics Journal* 34**:**323-334.

Starchev, K., Ricka, J. and Buffle, J. 2001. Noise on Fluorescence Correlation Spectroscopy. *Journal of Colloid and Interface Science* 233**:**50-55.

Steiner, R. F. 1991. Fluorescence Anisotropy: Theory and Applications. In *Topics in Fluorescence Spectroscopy: Techniques,* ed. J. R. Lakowicz, 1-52. New York: Springer.

Valeur, B. 2002. *Molecular Fluorescence: Principles and Applications.* Weinheim: Wiley-VCH.

Visser, N. V., Hink, M. A., Van Hoek, A. and Visser, A. 1999. Comparison between fluorescence correlation spectroscopy and time-resolved fluorescence anisotropy as illustrated with a fluorescent dextran conjugate. *Journal of Fluorescence* 9**:**251-255.

Volkmer, A., Subramaniam, V., Birch, D. J. S. and Jovin, T. M. 2000. One- and Two-Photon Excited Fluorescence Lifetimes and Anisotropy Decays of Green Fluorescent Proteins. *Biophysical Journal* 78**:**1589-1598.

Wang, X. F., Periasamy, A., Wodnicki, P., Gordon, G. and Herman, B. 1996. Time-resolved fluorescence lifetime imaging microscopy: Instrumentation and biomedical applications. In *Fluorescence Imaging Spectroscopy and Microscopy,* ed. X. F. Wang and B. Herman, 273-304. New York: John Wiley and Sons.

Wennmalm, S., Edman, L. and Rigler, R. 1997. Conformational fluctuations in single DNA molecules. *Proceedings of the National Academy of Sciences of the United States of America* 94**:**10641-10646.

Wetzel, R., Shivaprasad, S. and Williams, A. D. 2006. Plasticity of Amyloid Fibrills. *Biochemistry* 46**:**1-10.

Williams, R. M., Zipfel, W. R. and Webb, W. W. 2005. Interpreting Second-Harmonic Generation Images of Collagen I Fibrils. *Biophysical Journal* 88**:**1377-1386.

Wouters, F. S., Verveer, P. J. and Bastiaens, P. I. H. 2001. Imaging biochemistry inside cells. *Trends in Cell Biology* 11**:**203-211.

Wu, B., Chen, Y. and Muller, J. D. 2006. Dual-color time-integrated fluorescence cumulant analysis. *Biophysical Journal* 91**:**2687-2698.

Wu, B. and Muller, J. D. 2005. Time-Integrated Fluorescence Cumulant Analysis in Fluorescence Fluctuation Spectroscopy. *Biophys. J.* 89**:**2721-2735.

Xu, C. and Webb, W. W. 1991. Multiphoton Excitation of Molecular Fluorophores and Nonlinear Laser Microscopy. In *Topics in Fluorescence Spectroscopy: Nonlinear and Two-Photon Induced Fluorescence,* ed. J. R. Lakowicz and C. D. Geddes, 471-540. New York: Springer.

Xu, C., Zipfel, W. R., Shear, J. B., Williams, R. M. and Webb, W. W. 1996 Multiphoton fluorescence excitation: New spectral windows for biological nonlinear microscopy.

Proceedings of the National Academy of Sciences of the United States of America 93**:**10763 -10768.

Zhou, W. and Wang, Z. L. 2007. *Scanning microscopy for nanotechnology: techniques and applications.* New York: Springer.

Zipfel, W. R., Williams, R. M., Christie, R., Nikitin, A. Y., Hyman, B. T. and Webb, W. W. 2003. Live tissue intrinsic emission microscopy using multiphoton-excited native fluorescence and second harmonic generation. *Proceedings of the National Academy of Sciences of the United States of America* 100**:**7075-7080.